

# Endothelial Insulin Resistance Exacerbates Experimental Periodontitis

瀬々, 起朗

<https://hdl.handle.net/2324/7157315>

---

出版情報 : Kyushu University, 2023, 博士 (歯学), 課程博士  
バージョン :  
権利関係 :

# Endothelial Insulin Resistance Exacerbates Experimental Periodontitis

Journal of Dental Research  
1–10


© International Association for Dental, Oral, and Craniofacial Research and American Association for Dental, Oral, and Craniofacial Research 2023

Article reuse guidelines:

sagepub.com/journals-permissions

DOI: 10.1177/00220345231181539

journals.sagepub.com/home/jdr

T. Zeze<sup>1</sup>, T. Shinjo<sup>1</sup> , K. Sato<sup>1</sup>, Y. Nishimura<sup>1</sup>, M. Imagawa<sup>1</sup>, S. Chen<sup>1</sup>, A.-k. Ahmed<sup>1</sup>, M. Iwashita<sup>1</sup>, A. Yamashita<sup>1</sup>, T. Fukuda<sup>1</sup>, T. Sanui<sup>1</sup>, K. Park<sup>2</sup>, G.L. King<sup>2</sup>, and F. Nishimura<sup>1</sup>

## Abstract

Epidemiological studies suggest that the severity of periodontitis is higher in people with diabetes than in healthy individuals. Insulin resistance might play a crucial role in the pathogenesis of multiple diabetic complications and is reportedly induced in the gingiva of rodents with type 2 diabetes; however, the molecular mechanisms underlying the pathogenesis of diabetes-related periodontitis remain unclear. Therefore, we aimed to investigate whether endothelial insulin resistance in the gingiva may contribute to the pathogenesis of periodontitis as well as elucidate its underlying molecular mechanisms. We demonstrated that insulin treatment downregulated lipopolysaccharide (LPS)-induced or tumor necrosis factor  $\alpha$  (TNF $\alpha$ )-induced VCAM1 expression in endothelial cells (ECs) via the PI3K/Akt activating pathway, resulting in reduced cellular adhesion between ECs and leukocytes. Hyperglycemia-induced selective insulin resistance in ECs diminished the effect of insulin on LPS- or TNF $\alpha$ -stimulated VCAM1 expression. Vascular endothelial cell-specific insulin receptor knockout (VEIRKO) mice exhibited selective inhibition of the PI3K/Akt pathway in the gingiva and advanced experimental periodontitis-induced alveolar bone loss via upregulation of *Vcam1*, *Tnfa*, *Mcp-1*, *Rankl*, and neutrophil migration into the gingiva compared with that in the wild-type (WT) mice despite being free from diabetes. We also observed that insulin-mediated activation of FoxO1, a downstream target of Akt, was suppressed in the gingiva of VEIRKO and high-fat diet (HFD)-fed mice, hyperglycemia-treated ECs, and primary ECs from VEIRKO. Further analysis using ECs transfected with intact and mutated FoxO1, with mutations at 3 insulin-mediated phosphorylation sites (T24A, S256D, S316A), suggested that insulin-mediated regulation of VCAM1 expression and cellular adhesion of ECs with leukocytes was attenuated by mutated FoxO1 overexpression. These results suggest that insulin resistance in ECs may contribute to the progression of periodontitis via dysregulated VCAM1 expression and cellular adhesion with leukocytes, resulting from reduced activation of the PI3K/Akt/FoxO1 axis.

**Keywords:** VCAM-1, alveolar bone loss, forkhead box protein O1, cell adhesion molecules, type 2 diabetes, periodontal diseases

## Introduction

Insulin is the only hormone that lowers blood glucose levels in the body through glucose intake into cells. In addition, insulin can target and exert varying effects on multiple organs and tissues. Hyperglycemia and low-grade systemic inflammation may inhibit insulin signal transduction by modifying insulin receptor substrates, which contribute to peripheral insulin resistance (Batista et al. 2021). Type 2 diabetes mellitus is mainly caused by 2 primary factors: defective insulin secretion by pancreatic  $\beta$ -cells and the attenuation of response to insulin (Galicia-García et al. 2020). Therefore, insulin resistance is a characteristic pathological change in individuals with diabetes. Collectively, hyperglycemia, hyperlipidemia, chronic inflammation, and insulin resistance are major factors in the pathogenesis of diabetic complications, such as diabetic nephropathy and atherosclerosis (King 2008; DeFronzo et al. 2015).

Epidemiological studies have suggested that the prevalence and severity of periodontitis are higher in people with diabetes than in healthy individuals (Nelson et al. 1990; Seppälä et al. 1993; Firatli 1997). Basic studies using diet-induced and genetically obese and diabetic rodent models have confirmed

the exacerbation of experimental periodontitis compared with that in the lean controls (Amar et al. 2007; Muluke et al. 2016). Observational studies reported that people with higher Homeostatic Model Assessment for Insulin Resistance (HOMA-IR), an index of whole-body insulin resistance, have a higher risk of advanced periodontitis (Song et al. 2016; Andriankaja et al. 2018). A previous study reported that rats with obesity and mild diabetes exhibited insulin resistance in the gingiva and endothelial dysfunction (Mizutani et al. 2014), suggesting a possible association between the pathogenesis of periodontitis and obesity and diabetes. Recent studies using

<sup>1</sup>Section of Periodontology, Faculty of Dental Science, Kyushu University, Fukuoka, Japan

<sup>2</sup>Section of Vascular Cell Biology, Joslin Diabetes Center, Harvard Medical School, Boston, MA, USA

A supplemental appendix to this article is available online.

### Corresponding Author:

T. Shinjo, Section of Periodontology, Faculty of Dental Science, Kyushu University, Maidashi 3-1-1, Higashi-ku, Fukuoka, 812-8582, Japan.  
Email: takanori.shinjo@dent.kyushu-u.ac.jp

conditional insulin receptor knockout mice have revealed novel molecular mechanisms by which insulin resistance directly contributes to diabetic complications such as dementia and sarcopenia (Kulkarni et al. 1999; O'Neill et al. 2016; Cai et al. 2018). However, the molecular mechanisms underlying the association between insulin resistance and the exacerbation of periodontitis remain unclear.

Endothelial cells (ECs) mediate the migration and infiltration of leukocytes into inflammatory foci in response to bacterial infection and local inflammation. Insulin can downregulate vascular cell adhesion molecule 1 (VCAM1) in ECs, thereby protecting against atherosclerosis by regulating the cellular adhesion of ECs and leukocytes (Rask-Madsen et al. 2010; Park, Li et al. 2018). Insulin-induced Akt phosphorylation suppresses the transcriptional activity of forkhead box protein O1 (FoxO1) (Nakae et al. 1999), and FoxO1 upregulates VCAM1 expression in ECs (Abid et al. 2006). However, the role of insulin in downregulating CAMs such as VCAM1 in ECs during infectious inflammation remains unclear.

Therefore, we investigated the mechanisms by which insulin resistance in ECs contributes to the exacerbation of periodontitis by focusing on the action of insulin on VCAM1 in ECs during infection-mediated inflammation using VEIRKO mice.

## Materials and Methods

Details of cell culture, reagents, Western blotting, cell adhesion assay, hyperglycemia treatment, tartrate-resistant acid phosphatase (TRAP) staining, immunofluorescence stain, and cell transfection are described in the Appendix.

### Mice

We complied with the updated ARRIVE (Animal Research: Reporting of In Vivo Experiments) 2.0 guidelines for animal studies. All protocols for animal use and euthanasia (Appendix) were approved by the Institutional Animal Care and Use Committee of Kyushu University (A20-244-1 and A22-097-0).

### Ex Vivo Study

Ex vivo experiments using mouse gingiva were performed as previously described (Mizutani et al. 2014). In brief, the maxillary gingiva around the molars from wild-type (WT), vascular endothelial cell-specific insulin receptor knockout (VEIRKO), and high-fat diet (HFD)-fed mice was collected after 16 h of fasting, immediately immersed in Dulbecco's modified Eagle's medium (DMEM) containing 0.1% fetal bovine serum (FBS) in a 12-well plate, and incubated for 2 h under conditions of 5% CO<sub>2</sub> and 37°C. Insulin stimulation (100 nM) was performed for 10 min. The harvested gingiva was frozen with dry ice, ground with a hammer, and then homogenized in RIPA lysis buffer containing protease and phosphatase inhibitors (Appendix). Samples were used for Western blotting analysis.

### Ligature-Induced Periodontal Model in Mice

Experimental periodontitis was induced in mice, as previously reported (Shinjo et al. 2023).

### Reverse Transcriptional Quantitative Polymerase Chain Reaction

The protocol and primer sequences used in this study are described in Appendix Table 1.

### Isolation and Culture of Primary Endothelial Cells from Mice

Primary lung ECs were isolated from VEIRKO and WT mice (Rask-Madsen et al. 2010). Briefly, mouse lungs were digested with collagenase type I (Fujifilm Wako), and dissociated cells were cultured (passage 0) in DMEM-L (Sigma-Aldrich) with endothelial cell growth supplement (ECGS; Corning) and heparin sodium salt (Sigma-Aldrich) in an atmosphere of 5% CO<sub>2</sub> at 37°C. Outgrowth cells from lung tissue were collected and sorted using Dynabeads (Thermo Fisher Scientific) conjugated with intercellular adhesion molecule 2 (ICAM2) antibody (BD Pharmingen) to isolate endothelial cells (passage 1). The sorting step was repeated in the next passage (passage 2). Primary lung endothelial cells were used in passages 3 to 6.

### Statistical Analysis

Data are presented as mean ± standard deviation (SD). Comparisons between the 2 groups were performed using an unpaired Student's *t* test. One-way and 2-way analyses of variance (ANOVAs), followed by post hoc tests, were performed to compare multiple groups using GraphPad Prism8 software (GraphPad Software). Statistical significance was set at  $P < 0.05$ .

## Results

### Insulin Downregulates Lipopolysaccharide-Induced or Tumor Necrosis Factor $\alpha$ -Induced VCAM1 Expressions in TKD2 Cells via the PI3K-Akt Pathway

TKD2 cells expressed high levels of insulin receptor beta (IR $\beta$ ) (Appendix Fig. 1), and insulin induced phosphorylation of Akt and Erk in a dose-dependent manner (Appendix Fig. 2A). In TKD2 cells, insulin downregulated VCAM1 expression at basal condition (Fig. 1A, B), similar to a previous report (Rask-Madsen et al. 2010). Insulin pretreatment effectively suppressed lipopolysaccharide (LPS)-induced and tumor necrosis factor  $\alpha$  (TNF $\alpha$ )-induced VCAM1 expression at 100 nM but not intercellular adhesion molecule 1 (ICAM1) and E-selectin expression, by 33.2% and 22.7%, respectively (Fig. 1A, B, Appendix Fig. 2B, C, Appendix Fig. 3A, B). The IKK inhibitor BAY11-7082 and the p38 inhibitor SB203580 pretreatment

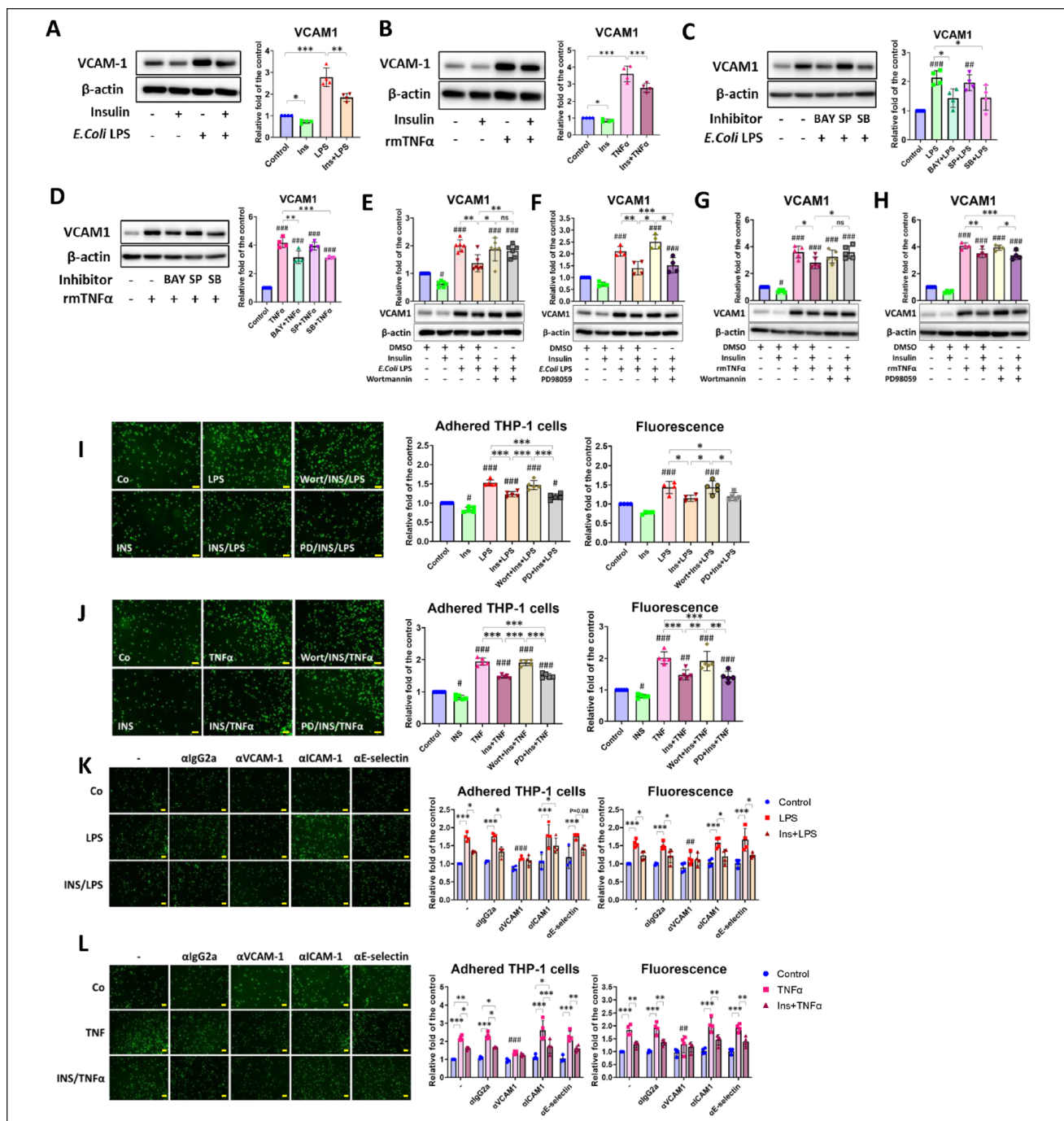


**Figure 1.** Insulin downregulated lipopolysaccharide (LPS)-induced or tumor necrosis factor  $\alpha$  (*TNF $\alpha$* )-induced vascular cell adhesion molecule 1 (VCAM1) expressions and cellular adhesion with leukocytes in TKD2 cells via the PI3K-Akt pathway. **(A)** LPS (10 ng/mL)-induced VCAM1 expressions in TKD2 cells with or without insulin (100 nM) pretreatment for 30 min. **(B)** *TNF $\alpha$*  (10 ng/mL)-induced VCAM1 expressions in TKD2 cells with or without insulin pretreatment for 30 min. **(C)** VCAM1 expression in LPS-stimulated TKD2 cells preincubated with IKK $\beta$  inhibitor BAY 11-7082 (10  $\mu$ M), JNK inhibitor SP600125 (10  $\mu$ M), or p38 inhibitor SB203580 (10  $\mu$ M) for 30 min. Cells treated with DMSO served as a control. **(D)** VCAM1 expression in *TNF $\alpha$* -stimulated TKD2 cells preincubated with BAY 11-7082, SP600125, or SB203580 for 30 min. **(E)** The levels of VCAM1 expression in LPS-stimulated TKD2 cells with or without incubation of a PI3K inhibitor wortmannin (100 nM). **(F)** The levels of VCAM1 expression in LPS *TNF $\alpha$* -treated TKD2 cells with or without incubation of an Erk inhibitor, PD98059 (10  $\mu$ M). **(G)** VCAM1 expression in *TNF $\alpha$* -treated TKD2 cells with or without incubation of a PI3K inhibitor wortmannin. **(H)** VCAM1 expression in *TNF $\alpha$* -treated TKD2 cells with or without incubation of PD98059. **(I)** Cellular adhesion of LPS-treated TKD2 cells with fluorescence-labeled THP-1 cells with insulin and inhibitors. **(J)** Cellular adhesion of *TNF $\alpha$* -treated TKD2 cells with fluorescence-labeled THP-1 cells with insulin and inhibitors. **(K)** Cellular adhesion of insulin and LPS-treated TKD2 cells with neutralizing antibodies against VCAM1, intercellular adhesion molecule 1 (ICAM1), and E-selectin (100 ng/mL). **(L)** Cellular adhesion of insulin and *TNF $\alpha$* -treated TKD2 cells with neutralizing antibodies against VCAM1, ICAM1, and E-selectin. The condition with isotype antibody ( $\alpha$ IgG2a, 100 ng/mL) was used as a control. Cells were stimulated with LPS or *TNF $\alpha$*  for 24 h. \* $P < 0.05$ . \*\* $P < 0.01$ . \*\*\* $P < 0.001$ . # $P < 0.05$ . ### $P < 0.01$ . #### $P < 0.001$  versus control, ns: no significance;  $n = 4-5$ . All individual data are shown in a scatterplot. Presentative microscopy photos are shown in Figure 1I to L. Scale bar = 100  $\mu$ m. Mean  $\pm$  SD is shown.

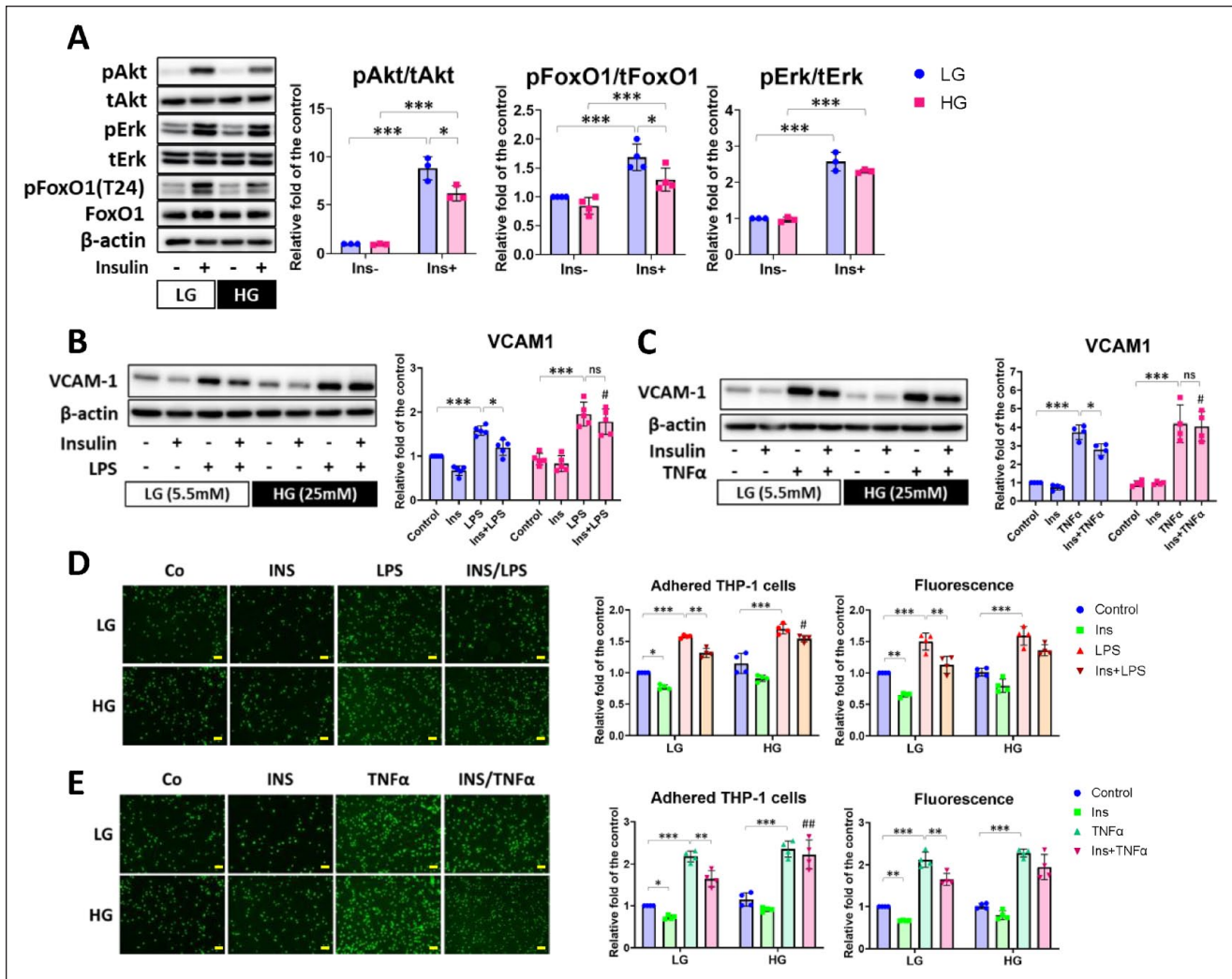


**Figure 2.** High glucose-induced selective insulin resistance mediates dysregulation of vascular cell adhesion molecule 1 (VCAM1) expressions in TKD2 cells. **(A)** Insulin signaling in TKD2 cells with or without insulin (100 nM) stimulation for 10 min under low glucose (LG; 5.5 mM D-glucose) or high glucose (HG; 25 mM D-glucose) for 48 h. **(B)** VCAM1 expression in TKD2 cells treated with lipopolysaccharide (LPS) (10 ng/mL) and/or insulin pretreatment for 30 min under LG or HG. **(C)** VCAM1 expression in TKD2 cells treated with tumor necrosis factor  $\alpha$  (TNF $\alpha$ ) (10 ng/mL) and/or insulin under LG or HG. **(D)** Cellular adhesion of TKD2 cells with THP-1 cells in the presence of insulin and/or LPS stimulation under LG or HG. **(E)** Cellular adhesion of TKD2 cells with THP-1 cells in the presence of insulin and/or TNF $\alpha$  stimulation under LG or HG. Cells were stimulated with LPS or TNF $\alpha$  for 24 h. \* $P < 0.05$ . \*\* $P < 0.01$ . \*\*\* $P < 0.001$ . # $P < 0.05$ . ## $P < 0.01$ . versus insulin + LPS under LG in B and D; ns, no significance;  $n = 3-5$ . All individual data are shown in a scatterplot. Representative Western blotting and microscopy photos are shown. Scale bar = 100  $\mu$ m. Data are expressed as mean  $\pm$  SD.

considerably downregulated LPS- and TNF $\alpha$ -induced VCAM1 expression in TKD2 cells. However, the c-Jun N-terminal kinase (JNK) inhibitor SP600125 did not alter the LPS- and TNF $\alpha$ -induced VCAM1 expression (Fig. 1C, D).

To confirm whether the PI3K-Akt or MAPK activation pathway was involved in the inhibitory effects of insulin on LPS- or TNF $\alpha$ -induced VCAM1 expression, TKD2 cells were treated with the PI3K inhibitor wortmannin or the MEK inhibitor PD98059 (Appendix Fig. 4A, B) before LPS or TNF $\alpha$  stimulation with or without insulin pretreatment. The inhibitory effects of insulin on LPS- or TNF $\alpha$ -induced VCAM1 expression in TKD2 cells were inhibited by wortmannin but not by PD98059 (Fig. 1E-H).

### *Insulin Suppresses Cellular Adhesion of LPS- or TNF $\alpha$ -Stimulated TKD2 Cells with Leukocytes via Downregulation of VCAM1 Expressions*

Next, to confirm whether insulin suppressed the cellular adhesion of TKD2 cells with leukocytes by regulating VCAM1 expression, the cellular adhesion assay was performed. Consistent with Western blotting data, cellular adhesion of LPS- and TNF $\alpha$ -stimulated TKD2 cells to THP-1 cells was significantly suppressed by insulin pretreatment, and these insulin effects were diminished by wortmannin but not by PD98059 (Fig. 1I-J). Neutralizing antibody against VCAM1 only blocked cellular adhesion of LPS- and TNF $\alpha$ -stimulated

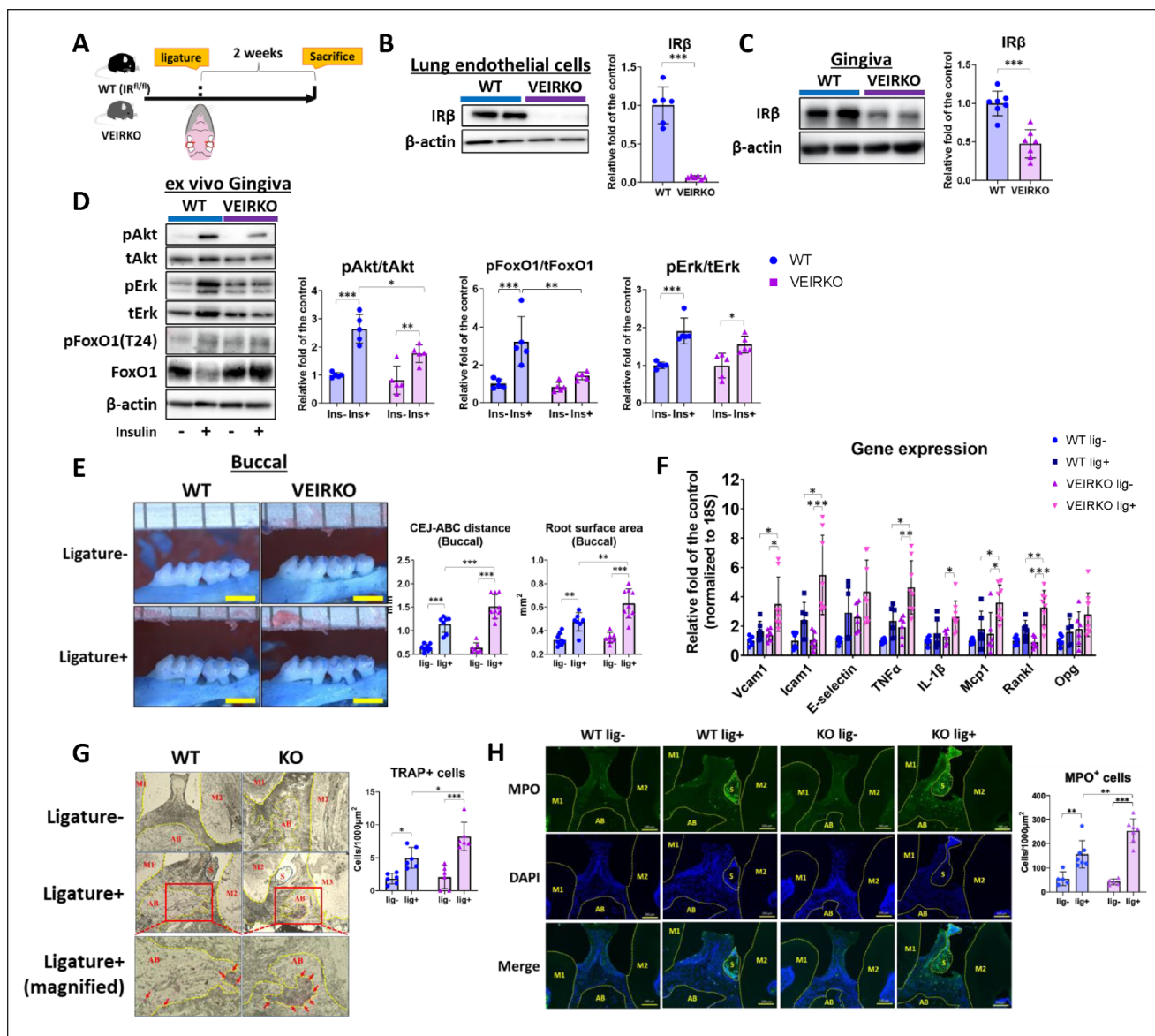


**Figure 3.** Vascular endothelial cell-specific insulin receptor knockout (VEIRKO) mice showed exacerbation of ligature-induced alveolar bone loss by increased leukocyte infiltration through vascular cell adhesion molecule 1 (VCAM1) upregulation. **(A)** A schematic of the experiment using wild-type (WT) and VEIRKO mice. **(B)** Insulin receptor beta (IR $\beta$ ) expression in primary lung endothelial cells (ECs) from WT and VEIRKO mice. **(C)** IR $\beta$  expression in primary lung ECs from WT and VEIRKO gingiva. **(D)** Insulin signaling in the gingiva from WT and VEIRKO mice with ex vivo insulin (100 nM) stimulation for 10 min. **(E)** Assessment of alveolar bone loss in WT and VEIRKO mice with or without ligature for 14 d. Scale bar = 1 mm. **(F)** Gene expressions in the gingiva from WT and VEIRKO mice with or without ligature for 14 d. **(G)** Tartrate-resistant acid phosphatase (TRAP) staining in the periodontal tissue of WT and VEIRKO mice with or without ligature for 14 d. Representative photos with 20- and 40-fold magnification are shown. **(H)** Detection of MPO-positive leukocytes in the periodontal tissue of WT and VEIRKO mice with or without ligature for 14 d. Scale bar = 100  $\mu$ m. AB, alveolar bone; M1, first molar; M2, second molar; M3, third molar; S, silk suture. \* $P < 0.05$ . \*\* $P < 0.01$ . \*\*\* $P < 0.001$ .  $n = 5-9$ . All individual data are shown in a scatterplot. Representative Western blotting and microscopy photos are shown. Data are expressed as mean  $\pm$  SD.

TKD2 cells with THP-1 cells, whereas insulin exerted an inhibitory effect on cellular adhesion under ICAM1 and E-selectin neutralization (Fig. 1K, L). In addition, insulin suppressed *Porphyromonas gingivalis*-derived LPS (PgLPS)- and Pam3CSK4-elicited VCAM1 expression in TKD2 cells, as well as subsequent cellular adhesion with THP-1 cells (Appendix Fig. 5A-E). Furthermore, insulin exhibited a similar effect on LPS or TNF $\alpha$ -treated b.End.3 cells, the brain endothelial cell line, as TKD2 cells (Appendix Fig. 6).

### High Glucose-Induced Selective Insulin Resistance Mediates Dysregulation of VCAM1 Expressions in TKD2 Cells

Hyperglycemia induced selective inhibition of the PI3K-Akt pathway on insulin signaling in ECs (Das Evcimen et al. 2007; Rask-Madsen and King 2007). Next, insulin signaling in TKD2 cells exposed to 25 mM D-glucose was assessed. Insulin-induced phosphorylation of Akt and its downstream FoxO1,

but not Erk, was significantly decreased by 29.7% and 22.9%, respectively, compared with that in the euglycemic condition (5.5 mM D-glucose) (Fig. 2A). Western blotting results revealed that the inhibitory effects of insulin on LPS- or TNF $\alpha$ -induced VCAM1 expression were attenuated under hyperglycemia (Fig. 2B, C). Similarly, hyperglycemia inhibited insulin-mediated downregulation of cellular adhesion between LPS- or TNF $\alpha$ -treated TKD2 and THP-1 cells (Fig. 2D, E). Insulin resistance did not occur following 20 mM mannitol treatment (Appendix Fig. 7A, B). HFD-fed mice showed mild diabetes (Appendix Fig. 8A–C) and consistent inhibition of insulin-induced Akt/FoxO1 phosphorylation in the gingiva (Appendix Fig. 8D).

### ***VEIRKO Mice Exhibited Exacerbation of Ligature-Induced Alveolar Bone Loss by Increased Infiltration of Leukocytes through VCAM1 Upregulation***

WT and VEIRKO mice were subjected to ligature-induced experimental periodontitis to assess the pathogenic role of insulin resistance in ECs during periodontitis (Fig. 3A). VEIRKO mice exhibited IR $\beta$  deficiency in primary lung ECs (Fig. 3B) and decreased IR $\beta$  expression in the gingiva by 53.6% compared with that in the WT mice (Fig. 3C). Consistent with a previous report (Konishi et al. 2017), VEIRKO mice showed lower IR $\beta$  expression in livers and lungs (Appendix Fig. 9A). Vascular ECs in periodontal tissue showed less IR $\beta$  expression in VEIRKO mice compared with WT mice (Appendix Fig. 9B).

We characterized insulin signaling in the gingiva of VEIRKO. Ex vivo insulin stimulation resulted in the phosphorylation of Akt, FoxO1, and Erk by 2.6-, 3.3-, and 1.9-fold in the gingiva of WT mice, respectively (Fig. 3D). By contrast, the ex vivo insulin-stimulated phosphorylation of Akt and FoxO1 in the gingiva of VEIRKO mice decreased by 33.0% and 59.2%, respectively, compared with that in WT mice, but Erk remained unchanged (Fig. 3D). Notably, ligature-induced alveolar bone loss in VEIRKO mice was significantly increased by 24.8% compared with that in WT mice (Fig. 3E). Quantitative polymerase chain reaction (qPCR) analysis suggested that *Vcam1*, *Icam1*, *Tnfa*, *Il1b*, *Mcp1*, *Rankl*, and *Opg* expression were significantly upregulated in the gingiva of ligated VEIRKO mice compared with that in ligated WT mice (Fig. 3F). The number of TRAP-positive cells in the periodontal tissue of ligated VEIRKO mice was significantly higher than that in ligated WT mice (Fig. 3G). Consistent with *Vcam1* upregulation, infiltration of MPO-positive cells was significantly increased in ligated VEIRKO mice compared with that in the ligated WT mice (Fig. 3H). HFD-fed mice showed increased alveolar bone loss and neutrophil infiltration by ligation compared with the control (Appendix Fig. 8E, F).

### ***Insulin-Mediated Regulation of LPS- or TNF $\alpha$ -Induced VCAM1 Expression Was Attenuated in Primary ECs from VEIRKO Mice***

To investigate the effect of reduced EC insulin receptors on VCAM1 expression, primary lung ECs from WT and VEIRKO

mice were used for an in vitro study. Insulin-mediated phosphorylation of Akt and FoxO1 significantly decreased in ECs from VEIRKO mice compared with that in ECs from WT mice, but insulin-induced Erk did not (Fig. 4A). The inhibitory effects of insulin on LPS- or TNF $\alpha$ -induced VCAM1 expression were diminished in ECs from VEIRKO mice, whereas LPS- or TNF $\alpha$ -stimulated VCAM1 expression was not enhanced by IR $\beta$  loss (Fig. 4B, C). In addition, insulin-mediated downregulation of cellular adhesion of LPS- or TNF $\alpha$ -treated ECs to leukocytes was abolished in VEIRKO mice (Fig. 4D, E).

### ***FoxO1 Is a Key Molecule for Insulin-Mediated Regulation of LPS- or TNF $\alpha$ -Induced VCAM1 Expression in ECs***

FoxO1 is involved in VCAM1-mediated cellular adhesion (Ferdous et al. 2011; Tsuchiya et al. 2012). The role of FoxO1 in insulin-mediated regulation of VCAM1 expression in LPS- or TNF $\alpha$ -stimulated TKD2 cells was investigated. We successfully overexpressed FLAG-tagged intact FoxO1 and FoxO1-ADA with mutations at 3 sites of insulin-mediated phosphorylation in TKD2 cells (Fig. 5A). FoxO1- and FoxO1-ADA-overexpressing TKD2 cells exhibited similar levels of insulin-induced phosphorylation of Akt and Erk compared with that in the control (Fig. 5B). FoxO1 activation by insulin was enhanced 2.8-fold in FoxO1-overexpressing cells compared with that in the control; however, it was substantially reduced in FoxO1-ADA-overexpressing cells (Fig. 5B). FoxO1 and FoxO1-ADA overexpression did not affect LPS- or TNF $\alpha$ -induced VCAM1 expression in TKD2 cells (Fig. 5C–E). However, insulin-mediated downregulation of LPS- or TNF $\alpha$ -stimulated VCAM1 expression was diminished in FoxO1-ADA-overexpressing TKD2 cells (Fig. 5C–E). Insulin did not affect the cellular adhesion of FoxO1-ADA-overexpressing TKD2 cells with or without LPS or TNF $\alpha$  stimulation (Fig. 5D–F).

## **Discussion**

The development of conditional IR knockout mice has helped elucidate the pathogenic role of insulin resistance in diabetes-related diseases and complications (Kulkarni et al. 1999; O'Neill et al. 2016; Cai et al. 2018). The regulatory effect of insulin on sterile inflammation-related VCAM1 expression in ECs reportedly prevented atherosclerosis in studies using vascular endothelial cell-specific IR knockout (VEIRKO) mice (Rask-Madsen et al. 2010). In this study, we demonstrated that insulin downregulates VCAM1 expression in ECs treated with *Escherichia coli* LPS and TNF $\alpha$  via the PI3K-Akt pathway, resulting in reduced leukocyte adhesion. We confirmed that hyperglycemia-induced selective inhibition of the PI3K-Akt pathway attenuated insulin-mediated downregulation of VCAM1 and adhesion with leukocytes in LPS- and TNF $\alpha$ -treated ECs. VEIRKO mice used in this study exhibited exacerbated alveolar bone loss and periodontal inflammation with upregulation of VCAM1 and neutrophil infiltration compared with that in WT littermates. We demonstrated that insulin-induced

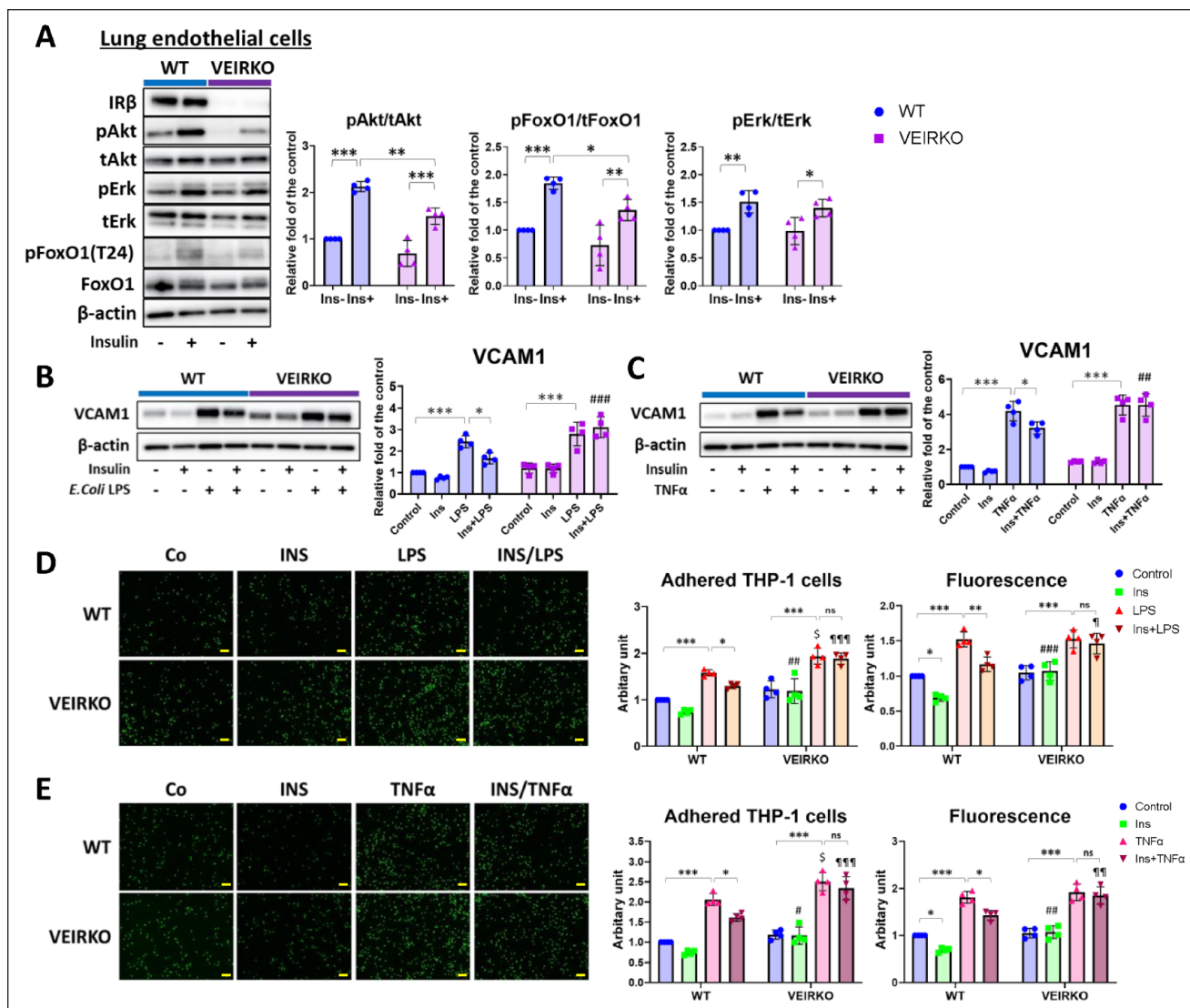


**Figure 4.** Insulin-regulated of lipopolysaccharide (LPS)-induced or tumor necrosis factor  $\alpha$  (TNF $\alpha$ )-induced vascular cell adhesion molecule 1 (VCAM1) expression was canceled in primary endothelial cells (ECs) from vascular endothelial cell-specific insulin receptor knockout (VEIRKO) mice. **(A)** Insulin signaling in primary lung ECs from wild-type (WT) and VEIRKO mice with insulin (100 nM) stimulation for 10 min. **(B)** VCAM1 expression in primary lung ECs from WT and VEIRKO mice treated with LPS (10 ng/mL) and/or insulin pretreatment for 30 min. **(C)** VCAM1 expression in primary lung ECs from WT and VEIRKO mice treated with TNF $\alpha$  (10 ng/mL) and/or insulin pretreatment for 30 min. **(D)** Cellular adhesion of primary lung ECs from WT and VEIRKO mice with THP-1 cells in the presence or absence of insulin pretreatment for 30 min and/or LPS stimulation. **(E)** Cellular adhesion of primary lung ECs from WT and VEIRKO mice with THP-1 cells in the presence or absence of insulin pretreatment for 30 min and/or TNF $\alpha$  stimulation. Cells were stimulated with LPS or TNF $\alpha$  for 24 h. \* $P$  < 0.05. \*\* $P$  < 0.01. \*\*\* $P$  < 0.001. # $P$  < 0.05. ## $P$  < 0.01. ### $P$  < 0.001 versus insulin + LPS in ECs from WT (B, C) versus insulin in ECs from WT (D, E); \$ $P$  < 0.05 versus LPS in ECs from WT (D, E); † $P$  < 0.05, †† $P$  < 0.01, ††† $P$  < 0.001 versus insulin + LPS or TNF $\alpha$  in ECs from WT (D, E); ns, no significance;  $n$  = 4. All individual data are shown in a scatterplot. Representative Western blotting and microscopy photos are shown. Scale bar = 100  $\mu$ m. Mean  $\pm$  SD is shown.

FoxO1 phosphorylation was decreased in the gingiva of both VEIRKO and HFD-fed WT mice, and ECs transfected with murine FoxO1 with mutations in 3 insulin-mediated phosphorylation sites revealed attenuated insulin-mediated action on endothelial VCAM1 expression and adhesion with leukocytes. HFD feeding causes hyperlipidemia, chronic inflammation, and hyperinsulinemia, resulting in systemic insulin resistance in mice (Heydemann 2016). Collectively, we confirmed that endothelial insulin resistance might contribute to the pathogenesis of periodontitis via dysregulation of VCAM1 and cellular adhesion in the gingiva. To the best of our knowledge, this is

the first study to show the inhibitory effect of insulin on endothelial cellular adhesion with leukocytes by suppressing LPS- or TNF $\alpha$ -induced VCAM1 expression via activation of the PI3K-Akt pathway (Fig. 1).

LPS- or TNF $\alpha$ -induced VCAM1 expression was dependent on both NF- $\kappa$ B and p38 activation (Fig. 1C, D) in TKD2 cells, suggesting that the PI3K-Akt pathway may regulate these activations. This finding is consistent with those of other studies reporting the involvement of p65 or p38 activation in VCAM1 expression in macrovascular ECs (Xia et al. 2014; Park, Kim et al. 2018). Among CAMs, neutralizing antibodies against



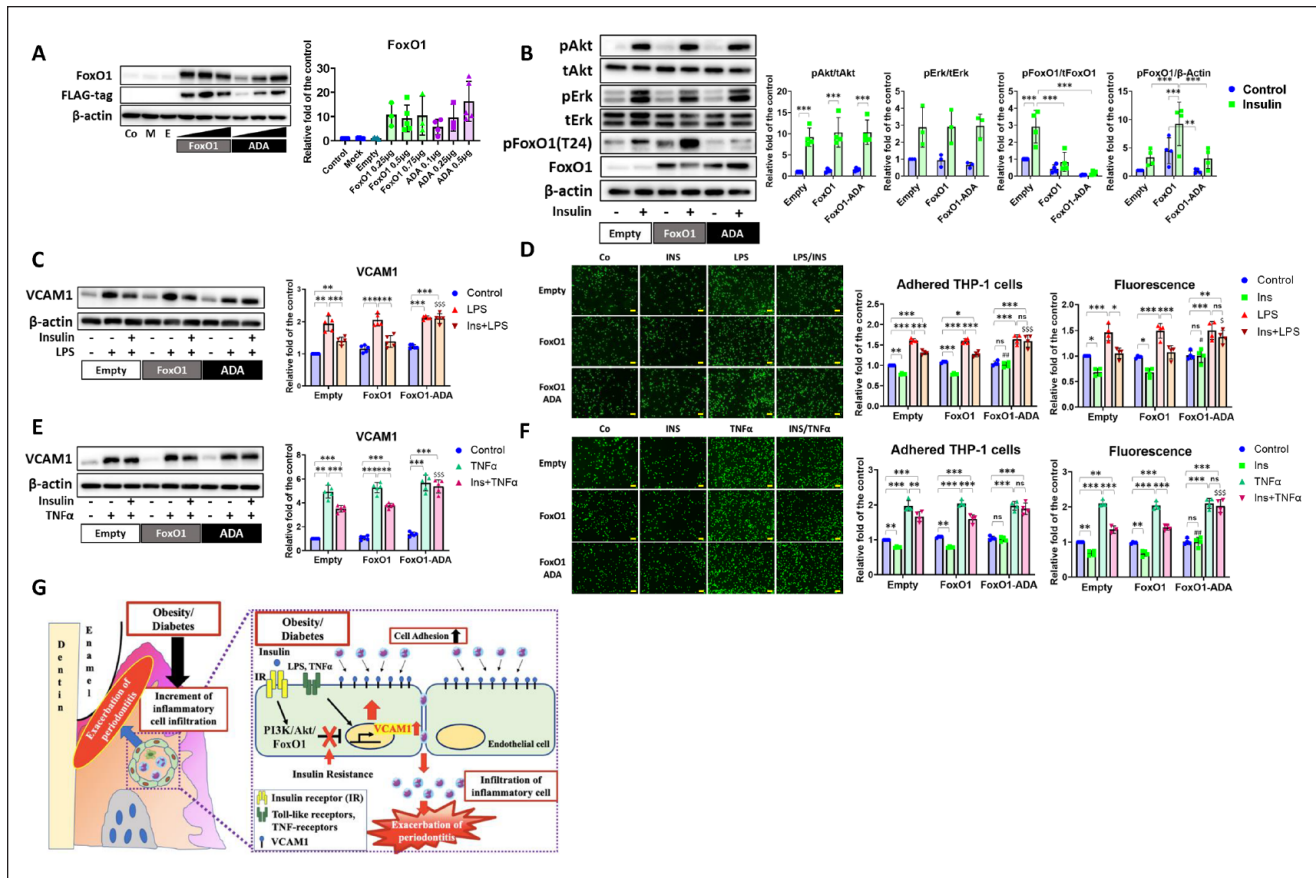


**Figure 5.** FoxO1 is the key molecule for insulin's regulation of lipopolysaccharide (LPS)-induced or tumor necrosis factor  $\alpha$  (TNF $\alpha$ )-induced vascular cell adhesion molecule 1 (VCAM1) expression in TKD2 cells. **(A)** Western blotting in TKD2 cells transfected with empty (E), intact FoxO1, and FoxO1-ADA plasmid at the indicated amount. No plasmid/Lipofectamine 3000 reagents served as control, and no plasmid with Lipofectamine 3000 served as mock (M). **(B)** Insulin signaling in TKD2 cells transfected with empty, intact FoxO1, and FoxO1-ADA plasmid (0.5  $\mu$ g each) with insulin (100 nM) stimulation for 10 min. **(C)** VCAM1 expression in TKD2 cells transfected with empty, intact FoxO1, and FoxO1-ADA plasmid treated with LPS (10 ng/mL) and/or insulin pretreatment for 30 min. **(D)** Cellular adhesion of TKD2 cells transfected with empty, intact FoxO1, and FoxO1-ADA plasmid with THP-1 cells in the presence or absence of LPS (10 ng/mL) and/or insulin pretreatment for 30 min. **(E)** VCAM1 expression in TKD2 cells transfected with empty, intact FoxO1, and FoxO1-ADA plasmid treated with TNF $\alpha$  (10 ng/mL) and/or insulin pretreatment for 30 min. **(F)** Cellular adhesion of TKD2 cells transfected with empty, intact FoxO1, and FoxO1-ADA plasmid with THP-1 cells in the presence or absence of TNF $\alpha$  (10 ng/mL) and/or insulin pretreatment for 30 min. **(G)** Summary of the findings in the present study. Cells were stimulated with LPS or TNF $\alpha$  for 24 h. \* $P < 0.05$ , \*\* $P < 0.01$ , \*\*\* $P < 0.001$ , # $P < 0.05$ , ## $P < 0.01$  versus insulin in TKD2 cells transfected with empty plasmid;  $\$P < 0.05$ , \$\$\$ $P < 0.001$  versus insulin + LPS in TKD2 cells transfected with FoxO1-ADA; ns, no significance;  $n = 4-5$ . All individual data are shown in a scatterplot. Representative Western blotting and microscopy photos are shown. Scale bar = 100  $\mu$ m. Mean  $\pm$  SD is shown.

VCAM1 only diminished the adhesion of LPS- or TNF $\alpha$ -stimulated TKD2 cells to THP-1 cells (Fig. 1K, L). The expression of VCAM1 and ICAM1 differs among endothelial cells derived from various tissues (Kanda et al. 1998). In addition, the differential roles of VCAM1 and ICAM1 reportedly depend on organs and tissues, such as the brain and skin (Norman et al. 2008). Concordantly, our findings confirmed that the expression of VCAM1, but not ICAM1 and E-selectin, was substantially induced by 10 ng/mL LPS or TNF $\alpha$  and that VCAM1 neutralization only blocked cellular adhesion with leukocytes in TKD2 cells.

FoxO1 may be involved in regulating VCAM1 expression in other cell types (Rask-Madsen et al. 2010; Almeida 2011; Ferdous et al. 2011; Tsuchiya et al. 2012). Therefore, we focused on the role of FoxO1 in LPS- or TNF $\alpha$ -induced

VCAM1 expression in ECs. Our results confirmed that hyperglycemia induces selective inhibition of the insulin-mediated phosphorylation of PI3K-Akt-FoxO1 in TKD2 cells, which attenuates insulin action on LPS- or TNF $\alpha$ -induced VCAM1 expression and subsequent cellular adhesion with leukocytes (Fig. 2). Hyperglycemia-induced insulin resistance is likely caused by oxidative stress-induced PKC-mediated phosphorylation of serine residues in insulin receptor substrates (Rask-Madsen and King 2007; Geraldine et al. 2009). These results suggest that hyperglycemia-induced selective insulin resistance dysregulates insulin-mediated VCAM1 expression related to LPS or TNF $\alpha$  stimulation.

The extent of ligature-induced alveolar bone loss observed in VEIRKO mice was comparable to that in HFD-fed mice, with insulin resistance in the gingiva and increased MPO-positive

cells (Fig. 3E, H and Appendix Fig. 8E, F), suggesting that insulin resistance in gingival ECs is an independent contributor to the progression of periodontitis. Ligatured-VEIRKO mice also showed upregulation of VCAM1 and ICAM1 in the gingiva (Fig. 3E, F), which might facilitate infiltration of inflammatory cells such as neutrophils and monocytes (Fig. 3F–H). Our results revealed that depletion of endothelial cell IR $\beta$  did not cause periodontal inflammation or basal bone destruction in VEIRKO mice, demonstrating the enhancement of periodontal inflammation by endothelial insulin resistance. These results suggest that VEIRKO mice exhibited exacerbation of ligature-induced experimental periodontitis owing to enhanced inflammation by increased leukocyte infiltration via endothelial insulin resistance, despite being free from obesity and diabetes.

We observed similar results in primary lung ECs of VEIRKO mice (Fig. 4), as noted in hyperglycemia-treated TKD2 cells (Fig. 2) exhibiting selective inhibition of insulin-induced phosphorylation of Akt- and FoxO1-dysregulated LPS- or TNF $\alpha$ -stimulated VCAM1 expression and cellular adhesion with leukocytes in ECs.

Finally, we confirmed that insulin-mediated phosphorylation of FoxO1 plays a critical role in the regulation of LPS- or TNF $\alpha$ -stimulated VCAM1 expression in ECs (Fig. 5). TKD2 cells overexpressing mutated FoxO1 were unresponsive to insulin (Fig. 5B), resulting in the loss of the suppression in VCAM1 expression and cellular adhesion with leukocytes in LPS- or TNF $\alpha$ -treated ECs (Fig. 5C–F). By contrast, overexpression of intact FoxO1 did not affect basal VCAM1 levels or enhance insulin-mediated regulation of VCAM1 expression (Fig. 5C, E). These results suggest that insulin-mediated phosphorylation of FoxO1 critically contributes to the inhibitory effect of insulin on VCAM1 expression during infectious inflammation. Growth factors, including insulin, activate FoxO1 in an Akt-dependent manner with phosphorylation at Thr26, Ser253, and Ser316, leading to nuclear export (Accili and Arden 2004). Oxidative stress can result in phosphorylation of FoxO1 at various sites different from insulin via JNK or macrophage stimulating 1 (MST1) (Almeida 2011; Ouyang and Li 2011). FoxO1 could also bind to the promoter region of VCAM1, indicating that FoxO1 activation might decrease the transcriptional activity of VCAM1 (Ferdous et al. 2011). In addition, mammalian cells possess FoxO3a and 4, which are also activated by insulin and participate in cellular function and biological processes (Almeida 2011; Ouyang and Li 2011). Further studies must be conducted to elucidate the involvement of other members of the FoxO family in inflammation-related CAM expression.

Several studies using human umbilical vein endothelial cells and rat artery ECs showed opposite effects of insulin action on cytokine-induced VCAM1 expression compared to our findings (Madonna et al. 2007; Pott et al. 2016). We considered that this was due to the difference in the origin of ECs since we used ECs derived from microvessel/capillaries in contrast to great vessel. Cellular functions and profiles in ECs could differ depending on vascular types (Trimm and Red-Horse 2023).

Our study has 4 major limitations. First, we cannot exclude the involvement of other mechanistic targets downstream of Akt, such as mechanistic target of rapamycin complex (mTORC) and glycogen synthase kinase 3 $\beta$  (GSK3 $\beta$ ), just by using VEIRKO mice. Therefore, EC-specific FoxO1 knockout mice would be helpful for elucidating the precise role of FoxO1 in the pathogenesis of periodontitis under insulin resistance and diabetes. Second, our results cannot indicate a therapeutic target and approach for diabetes-related periodontitis. Future studies should examine whether enhanced insulin signaling prevents the progression of periodontitis under diabetes or insulin resistance. Third, in the absence of established methods to isolate and culture ECs from the gingiva, we used a renal endothelial cell line TKD2 since fenestrated capillaries include kidney vascular ECs and gingival ECs (Tsubokawa and Sato 2014; Hennigs et al. 2021); future studies using primary or cell lines of gingival ECs to confirm the findings in the present study are needed. Fourth, future studies using severe type 2 diabetes model mice such as db/db mice should be conducted since HFD-fed mice showed mild obesity.

In conclusion, we demonstrated that insulin could down-regulate LPS- or TNF $\alpha$ -induced VCAM1 expression in ECs and subsequent cellular adhesion to leukocytes, and insulin resistance caused by obesity or diabetes might dysregulate insulin action, leading to exacerbated periodontal inflammation and alveolar bone loss via inhibition of the PI3K/Akt/FoxO1 pathway in ECs (Fig. 5G).

### Author Contributions

T. Zeze, contributed to data acquisition, analysis, and interpretation, drafted the manuscript; T. Shinjo, contributed to conception and design, data acquisition, analysis, and interpretation, drafted the manuscript; K. Sato, Y. Nishimura, M. Imagawa, S. Chen, A.-k. Ahmed, contributed to data acquisition, critically revised the manuscript; M. Iwashita, A. Yamashita, T. Fukuda, T. Sanui, K. Park, G.L. King, contributed to data interpretation, critically revised the manuscript; F. Nishimura, contributed to data analysis and interpretation, critically revised manuscript. All authors gave their final approval and agreed to be accountable for all aspects of the work.

### Acknowledgments

We are grateful for the support of Dr. C. Ronald Kahn at the Joslin Diabetes Center (JDC) for IR-floxed mice. In addition, we are grateful for the technical assistance provided by the Research Support Center and Research Center for Human Disease Modeling at Kyushu University Graduate School of Medical Sciences. T. Shinjo is a recipient of the Kaneda Hiroo Fellowship from Sunstar Foundation. A.-k. Ahmed is a recipient of the Japanese Government (MEXT) Scholarship. We also thank Editage ([www.editage.com](http://www.editage.com)) for English language editing.

### Declaration of Conflicting Interests

The authors declared no potential conflicts of interest with respect to the research, authorship, and/or publication of this article.

## Funding

The authors disclosed receipt of the following financial support for the research, authorship, and/or publication of this article: This study was supported by Japan Society for the Promotion of Science (JSPS) KAKENHI JP20K18513 (T. Shinjo) and Japan Science and Technology Agency (JST) SPRING JPMJSP2136 (T. Zeze).

## ORCID iD

T. Shinjo  <https://orcid.org/0000-0002-8269-2826>

## Data Availability

All data published in the present article are available upon reasonable request.

## References

- Abid MR, Shih SC, Otu HH, Spokes KC, Okada Y, Curiel DT, Minami T, Aird WC. 2006. A novel class of vascular endothelial growth factor-responsive genes that require forkhead activity for expression. *J Biol Chem*. 281(46):35544–35553.
- Accili D, Arden KC. 2004. FoxOs at the crossroads of cellular metabolism, differentiation, and transformation. *Cell*. 117(4):421–426.
- Almeida M. 2011. Unraveling the role of FoxOs in bone—insights from mouse models. *Bone*. 49(3):319–327.
- Amar S, Zhou Q, Shaik-Dasthagirisaheb Y, Leeman S. 2007. Diet-induced obesity in mice causes changes in immune responses and bone loss manifested by bacterial challenge. *Proc Natl Acad Sci U S A*. 104(51):20466–20471.
- Andriankaja OM, Muñoz-Torres FJ, Vivaldi-Oliver J, Leroux BG, Campos M, Josphipura K, Pérez CM. 2018. Insulin resistance predicts the risk of gingival/periodontal inflammation. *J Periodontol*. 89(5):549–557.
- Batista TM, Haider N, Kahn CR. 2021. Defining the underlying defect in insulin action in type 2 diabetes. *Diabetologia*. 64(5):994–1006.
- Cai W, Xue C, Sakaguchi M, Konishi M, Shirazian A, Ferris HA, Li ME, Yu R, Kleinridders A, Pothos EN, et al. 2018. Insulin regulates astrocyte gliotransmission and modulates behavior. *J Clin Invest*. 128(7):2914–2926.
- Das Evcimen N, King GL. 2007. The role of protein kinase C activation and the vascular complications of diabetes. *Pharmacol Res*. 55(6):498–510.
- DeFronzo RA, Ferrannini E, Groop L, Henry RR, Herman WH, Holst JJ, Hu FB, Kahn CR, Raz I, Shulman GI, et al. 2015. Type 2 diabetes mellitus. *Nat Rev Dis Primers*. 1:15019.
- Ferdous A, Morris J, Abedin MJ, Collins S, Richardson JA, Hill JA. 2011. Forkhead factor FoxO1 is essential for placental morphogenesis in the developing embryo. *Proc Natl Acad Sci U S A*. 108(39):16307–16312.
- Firatli E. 1997. The relationship between clinical periodontal status and insulin-dependent diabetes mellitus. Results after 5 years. *J Periodontol*. 68(2):136–140.
- Galicia-Garcia U, Benito-Vicente A, Jebari S, Larrea-Sebal A, Siddiqi H, Uribe KB, Ostolaza H, Martín C. 2020. Pathophysiology of type 2 diabetes mellitus. *Int J Mol Sci*. 21(17):6275.
- Geraldes P, Hiraoka-Yamamoto J, Matsumoto M, Clermont A, Leitges M, Marette A, Aiello LP, Kern TS, King GL. 2009. Activation of PKC-delta and SHP-1 by hyperglycemia causes vascular cell apoptosis and diabetic retinopathy. *Nat Med*. 15(11):1298–1306.
- Hennigs JK, Matuszcak C, Trepel M, Körbelin J. 2021. Vascular endothelial cells: heterogeneity and targeting approaches. *Cells*. 10(10):2712.
- Heydemann A. 2016. An overview of murine high fat diet as a model for type 2 diabetes mellitus. *J Diabetes Res*. 2016:2902351.
- Kanda K, Hayman GT, Silverman MD, Lelkes PI. 1998. Comparison of ICAM-1 and VCAM-1 expression in various human endothelial cell types and smooth muscle cells. *Endothelium*. 6(1):33–44.
- King GL. 2008. The role of inflammatory cytokines in diabetes and its complications. *J Periodontol*. 79(8 Suppl):1527–1534.
- Konishi M, Sakaguchi M, Lockhart SM, Cai W, Li ME, Homan EP, Rask-Madsen C, Kahn CR. 2017. Endothelial insulin receptors differentially control insulin signaling kinetics in peripheral tissues and brain of mice. *Proc Natl Acad Sci USA*. 114(40):E8478–E8487.
- Kulkarni RN, Brüning JC, Winnay JN, Postic C, Magnuson MA, Kahn CR. 1999. Tissue-specific knockout of the insulin receptor in pancreatic beta cells creates an insulin secretory defect similar to that in type 2 diabetes. *Cell*. 96(3):329–339.
- Madonna R, Massaro M, Pandolfi A, Consoli A, De Caterina R. 2007. The prominent role of p38 mitogen-activated protein kinase in insulin-mediated enhancement of VCAM-1 expression in endothelial cells. *Int J Immunopathol Pharmacol*. 20(3):539–555.
- Mizutani K, Park K, Mima A, Katagiri S, King GL. 2014. Obesity-associated gingival vascular inflammation and insulin resistance. *J Dent Res*. 93(6):596–601.
- Muluke M, Gold T, Kieffhaber K, Al-Sahli A, Celenti R, Jiang H, Cremers S, Van Dyke T, Schulze-Späte U. 2016. Diet-induced obesity and its differential impact on periodontal bone loss. *J Dent Res*. 95(2):223–229.
- Nakae J, Park BC, Accili D. 1999. Insulin stimulates phosphorylation of the forkhead transcription factor FKHR on serine 253 through a wortmannin-sensitive pathway. *J Biol Chem*. 274(23):15982–15985.
- Nelson RG, Shlossman M, Budding LM, Pettitt DJ, Saad MF, Genco RJ, Knowler WC. 1990. Periodontal disease and NIDDM in Pima Indians. *Diabetes Care*. 13(8):836–840.
- Norman MU, James WG, Hickey MJ. 2008. Differential roles of ICAM-1 and VCAM-1 in leukocyte-endothelial cell interactions in skin and brain of MRL/fas<sup>lpr</sup> mice. *J Leukoc Biol*. 84(1):68–76.
- O'Neill BT, Lee KY, Klaus K, Softic S, Krumpoch MT, Fentz J, Stanford KI, Robinson MM, Cai W, Kleinridders A, et al. 2016. Insulin and IGF-1 receptors regulate FoxO-mediated signaling in muscle proteostasis. *J Clin Invest*. 126(9):3433–3446.
- Ouyang W, Li MO. 2011. Foxo: in command of T lymphocyte homeostasis and tolerance. *Trends Immunol*. 32(1):26–33.
- Park K, Li Q, Evcimen ND, Rask-Madsen C, Maeda Y, Maddaloni E, Yokomizo H, Shinjo T, St-Louis R, Fu J, Gordin D, et al. 2018. Exogenous insulin infusion can decrease atherosclerosis in diabetic rodents by improving lipids, inflammation, and endothelial function. *Arterioscler Thromb Vasc Biol*. 38(1):92–101.
- Park KH, Kim J, Lee EH, Lee TH. 2018. Cynandione A inhibits lipopolysaccharide-induced cell adhesion via suppression of the protein expression of VCAM-1 in human endothelial cells. *Int J Mol Med*. 41(3):1756–1764.
- Pott GB, Tsurudome M, Bamfo N, Goalstone ML. 2016. ERK2 and Akt are negative regulators of insulin and tumor necrosis factor- $\alpha$  stimulated VCAM-1 expression in rat aorta endothelial cells. *J Inflamm (Lond)*. 13:6.
- Rask-Madsen C, King GL. 2007. Mechanisms of disease: endothelial dysfunction in insulin resistance and diabetes. *Nat Clin Pract Endocrinol Metab*. 3(1):46–56.
- Rask-Madsen C, Li Q, Freund B, Feather D, Abramov R, Wu IH, Chen K, Yamamoto-Hiraoka J, Goldenbogen J, Sotiropoulos KB, et al. 2010. Loss of insulin signaling in vascular endothelial cells accelerates atherosclerosis in apolipoprotein E null mice. *Cell Metab*. 11(5):379–389.
- Seppälä B, Seppälä M, Ainamo J. 1993. A longitudinal study on insulin-dependent diabetes mellitus and periodontal disease. *J Clin Periodontol*. 20(3):161–165.
- Shinjo T, Onizuka S, Zaito Y, Ishikado A, Park K, Li Q, Yokomizo H, Zeze T, Sato K, St-Louis R, et al. 2023. Dysregulation of CXCL1 expression and neutrophil recruitment in insulin resistance and diabetes-related periodontitis in male mice. *Diabetes* [epub ahead of print 14 Apr 2023]. doi:10.2337/db22-1014.
- Song IS, Han K, Park YM, Ji S, Jun SH, Ryu JJ, Park JB. 2016. Severe periodontitis is associated with insulin resistance in non-abdominal obese adults. *J Clin Endocrinol Metab*. 101(11):4251–4259.
- Trimm E, Red-Horse K. 2023. Vascular endothelial cell development and diversity. *Nat Rev Cardiol*. 20(3):197–210.
- Tsubokawa M, Sato S. 2014. In vitro analysis of human periodontal microvascular endothelial cells. *J Periodontol*. 85(8):1135–1142.
- Tsuchiya K, Tanaka J, Shuiqing Y, Welch CL, DePinho RA, Tabas I, Tall AR, Goldberg IJ, Accili D. 2012. FoxOs integrate pleiotropic actions of insulin in vascular endothelium to protect mice from atherosclerosis. *Cell Metab*. 15(3):372–381.
- Xia F, Wang C, Jin Y, Liu Q, Meng Q, Liu K, Sun H. 2014. Luteolin protects HUVECs from TNF- $\alpha$ -induced oxidative stress and inflammation via its effects on the Nox4/ROS-NF- $\kappa$ B and MAPK pathways. *J Atheroscler Thromb*. 21(8):768–783.

1 **Appendix materials**

2  
3 Title: Endothelial insulin resistance exacerbates experimental periodontitis

4  
5 Tatsuro Zeze<sup>1</sup>, Takanori Shinjo<sup>1</sup>, Kohei Sato<sup>1</sup>, Yuki Nishimura<sup>1</sup>, Mio Imagawa<sup>1</sup>, Shuang  
6 Chen<sup>1</sup>, Al-kafee Ahmed<sup>1</sup>, Misaki Iwashita<sup>1</sup>, Akiko Yamashita<sup>1</sup>, Takao Fukuda<sup>1</sup>,  
7 Terukazu Sanui<sup>1</sup>, Kyoungmin Park<sup>2</sup>, George L King<sup>2</sup>, Fusanori Nishimura<sup>1</sup>

8  
9 <sup>1</sup>Section of Periodontology, Faculty of Dental Science, Kyushu University, Fukuoka, Japan

10 <sup>2</sup>Section of Vascular Cell Biology, Joslin Diabetes Center, Harvard Medical School, Boston,  
11 Massachusetts

12  
13 \*Corresponding Author: Takanori Shinjo, Section of Periodontology, Faculty of Dental Science,  
14 Kyushu University, Fukuoka, Japan, Maidashi 3-1-1, Higashi-ku, Fukuoka, Fukuoka, Japan,  
15 Tel: +8192-642-6358 Fax: +8192-642-6360. Email: [takanori.shinjo@dent.kyushu-u.ac.jp](mailto:takanori.shinjo@dent.kyushu-u.ac.jp)

16  
17 Keywords: VCAM-1, Alveolar bone loss, Forkhead Box Protein O1, Cell Adhesion Molecules,  
18 Type 2 Diabetes, Periodontal Diseases

19 **Materials and methods**

20

21 **Cell culture**

22 The murine renal microvascular endothelial cell line TKD2 (IFO50374) was purchased from the  
23 Japanese Collection of Research Bioresources Cell Bank (JCRB; Osaka, Japan). TKD2 cells were  
24 cultured in the specific medium as JCRB instructed: Dulbecco's modified Eagles medium with low  
25 glucose (DMEM-L; Sigma-Aldrich, St. Louis, MO, USA) containing 2% FBS, 1  $\mu$ M insulin (Sigma-  
26 Aldrich), ethanolamine (Sigma-Aldrich), and recombinant mouse (rm) epidermal growth factor (EGF;  
27 Bio Legend, San Diego, CA, USA) in an atmosphere of 5% CO<sub>2</sub> at 33 °C.

28 The human monocytic leukemia cell line THP-1 (RCB1189) was purchased from RIKEN BioResource  
29 Center (Ibaraki, Japan) and maintained in Roswell Park Memorial Institute (RPMI) 1640 medium  
30 (Nacalai Tesque, Kyoto, Japan) containing 10% FBS (Biowest, Vieux Bourg, France), penicillin-  
31 streptomycin (Nacalai Tesque), and GlutaMAX (Life Technologies Corporation, Grand Island, NY,  
32 USA).

33 Murine 3T3-L1 preadipocytes (ATCC, Manassas, VA, USA) were differentiated into adipocytes using  
34 differentiation medium containing 4  $\mu$ g/ml dexamethasone, 0.5 mM 3-isobutyl-1-methylxanthine, 200  
35 nM insulin, and 10% FBS for 48 h as previously reported (Shinjo et al. 2015). Then, cells were cultured  
36 in DMEM supplemented with 10% FBS and 1  $\mu$ M insulin every other day and used for experiments  
37 as mature adipocytes on day 12 after the induction of differentiation. A mouse brain microvascular  
38 derived endothelial cell line, b.End.3 cell (CRL-2299), was obtained from ATCC and cultured in  
39 DMEM-L supplemented with 10% FBS and penicillin-streptomycin in an atmosphere of 5% CO<sub>2</sub> at  
40 37 °C.

41

42 **Reagents**

43 The antibodies against VCAM-1 (ab134047) were purchased from Abcam (Cambridge, UK), anti-  
44 ICAM-1 (sc-8439), E-Selectin (sc-137054) antibodies were purchased from Santa Cruz  
45 Biotechnology (Dallas, TX, USA), anti-insulin receptor  $\beta$  (#3025), phospho-Akt (Ser473) (#9271),  
46 total Akt (#4691), phospho-Erk (4370P), total Erk (#9102), phospho-FoxO1 (Thr24)/FoxO3a (Thr32)  
47 (#9464), and total FoxO1 (#2880) antibodies were obtained from Cell Signaling Technology (Danvers,  
48 CO, USA). An antibody against  $\beta$ -actin (010-27841) was purchased from Fuji-film Wako (Osaka,  
49 Japan). Secondary antibodies against horseradish peroxidase (HRP)-linked anti-mouse IgG (#7076)  
50 and HRP-linked anti-Rabbit IgG (#7074) were obtained from Cell Signaling Technology. PI3K  
51 inhibitor wortmannin (HY-10197), MEK inhibitor PD98059 (HY-12028), IKK inhibitor BAY-11-7082  
52 (HY-13453), JNK inhibitor SP600125 (HY-12041), and p38 inhibitor SB203580 (HY-10256) were  
53 purchased from MedChemExpress (New Jersey, USA). *E. coli* LPS (O111:B4, L4391) and insulin  
54 (I1882) were purchased from Sigma-Aldrich. Lipopolysaccharide from *Porphyromonas gingivalis*

55 (tlrl-pglps) and Pam3CSK4 (tlrl-pms) were obtained from InvivoGen (San Diego, CA, USA). rmTNF $\alpha$   
56 (MT-410) was purchased from the R&D System (Minneapolis, MN, USA). Neutralizing antibodies  
57 against IgG2a (14-4321-82), VCAM-1 (14-1061-82), ICAM-1 (14-0541-82), and E-Selectin (MA1-  
58 06507) were obtained from Thermo Fisher Scientific (Waltham, MA, USA). An antibody against  
59 myeloperoxidase (MPO; ab208670), and goat anti-rabbit IgG conjugated with Alexa Flour® 488  
60 (ab150077) were purchased from Abcam. Anti-mouse CD31 antibody was purchased from Bio Legend.  
61 An rabbit monoclonal antibody against IR $\beta$  (#23413) was obtained from Cell Signaling Technology.  
62 Secondary antibodies against mouse and rabbit IgG conjugated with Alexa Fluor 562 and 488 were  
63 purchased from Jackson ImmunoResearch Inc. (West Grove, PA, USA). All other reagents were of  
64 analytical grade. Dilutions used for each application are listed in Appendix Table 1.

65

### 66 **Western blotting analysis**

67 TKD2 cells and b.End.3 cells ( $1.0 \times 10^5$  cells, respectively) were cultured in 12-well plates for 48 h.  
68 After 24-h culturing in DMEM-L supplemented with 0.1% FBS, cells were pretreated with 100 nM  
69 insulin or PBS for 30 min, and stimulated with 10 ng/ml *Escherichia coli* LPS (Since mice with  
70 ligature-induced periodontitis showed persistent dysbiosis in the oral microbiome with a relative  
71 increase in Enterobacteriaceae, *E. coli* LPS was used for the *in vitro* study as a representative stimulus  
72 derived from bacteria (Kitamoto et al., 2020) or TNF $\alpha$  (we used TNF $\alpha$  as a representative  
73 inflammatory cytokine in periodontitis since several papers have reported that TNF $\alpha$  potently induces  
74 VCAM1 in ECs) for 24 h. For studies using inhibitors, each inhibitor was added to TKD2 cells 30 min  
75 before insulin pretreatment. Cells were collected in ice-cold RIPA lysis buffer (Nacalai Tesque)  
76 supplemented with protease inhibitor mixture (1:100 dilution; 25955-11, Nacalai Tesque) and  
77 phosphatase inhibitor mixture (1:100 dilution; 78428, Sigma-Aldrich), then homogenized. For the *ex*  
78 *vivo* study, the harvested gingiva were snap frozen with dry ice, ground with a hammer, then  
79 homogenized in RIPA buffer containing protease and phosphatase inhibitors as mentioned above.  
80 Collected liver and lung tissues were frozen, ground, and homogenized as well. Protein concentrations  
81 were determined using the BCA Protein assay kit (Thermo Fisher Scientific). Lysates with a fixed  
82 protein concentration were subjected to SDS/PAGE, then gels were transferred to PVDF membranes.  
83 After blocking with 5% skim milk or 5% BSA, membranes were incubated with primary antibodies at  
84 4 °C overnight and with appropriate secondary antibodies for 1 h. Membranes were developed using  
85 a chemiluminescent Chemi-Lumi One Super (02230-30; Nacalai Tesque). Blots were scanned using  
86 Image Quant LAS800 (GE healthcare, Chicago, IL, USA) and analyzed using ImageJ software  
87 (National Institute of Health, Bethesda, MA, USA). Antibody concentrations for western blotting  
88 (WB) are listed in Appendix Table 2. Unedited WB gels are shown in another Supplemental Material.

89

### 90 **Cell adhesion assay**

91 The CytoSelect™ Leukocyte-endothelium Adhesion Assay was purchased from Cell Biolab (San  
92 Diego, CA, USA) and performed according to the manufacturer's instructions. TKD2 and mouse lung  
93 endothelial cells were plated on a 96-well plate and stimulated under the same conditions as western  
94 blotting. After that, the cells were washed twice with serum-free RPMI1640, and pre-fluorescently  
95 labeled THP-1 cells were sprinkled and incubated for 30 min. Then, after washing three times with a  
96 dedicated wash buffer, 5 images of adhered THP-1 cells per well were taken using an All-in-One  
97 Fluorescence Microscope BZ-X800 (Keyence, Osaka, Japan). The number of adhered cells was  
98 counted based on the captured images and fluorescence intensity was measured using Enight™  
99 multimode plate reader (PerkinElmer, Waltham, MA, USA). For neutralization and inhibitor  
100 treatments, each neutralizing antibody or inhibitor was added to TKD2 cells 60 min before insulin  
101 treatment.

102

### 103 **Mouse studies**

104 IR-floxed (IR<sup>fl/fl</sup>) mice and vascular endothelial (VE)-cadherin-Cre recombinase transgenic mice  
105 [B6.FVB-Tg (Cdh5-cre)7Mlia/J; Jackson Laboratories, Bar Harbor, ME, USA] were used to generate  
106 endothelial-specific IR knockout mice (VE-cadherin-Cre<sup>+/-</sup>:IR<sup>fl/fl</sup>; VEIRKO) and wild-type (VE-  
107 cadherin-Cre<sup>-/-</sup>: IR<sup>fl/fl</sup>; WT) littermates. VE-cadherin-Cre transgenic mice were backcrossed with  
108 C57BL/6 mice for 12 generations before arriving at Jackson Laboratories and bred with C57BL/6J  
109 inbred mice at Jackson Laboratories for at least one generation to establish a colony. The colonies  
110 were maintained by breeding mice together. The IR<sup>fl/fl</sup> mice used in this study were backcrossed for  
111 over 10 generations with C57BL/6 mice before the initiation of these experiments. Genotyping was  
112 performed using DNA isolated from mice using primers, as shown in Appendix Table 1. Six-week-old  
113 male WT mice were fed a 60% high-fat diet (HFD; Oriental East, Tokyo, Japan) for 10 weeks. WT  
114 mice were used as a control. WT and VEIRKO mice were co-housed in a cage during experiments.  
115 All mice were housed under climate-controlled conditions with a 12-h light/dark cycle and with food  
116 and water *ad libitum*. To confirm IRβ expression in multiple organs, liver and lung were collected and  
117 used for western blotting. We used 58 WT mice, 48 VEIRKO and 40 HFD-fed mice (of which we  
118 excluded 10 WT, 10 VEIRKO and 4 HFD-fed mice due to failure in ligation or lung EC isolation) for  
119 the entire study.

120

### 121 **Induction of ligature-induced periodontitis in mice**

122 WT (14-week-old males), VEIRKO, and HFD-fed mice were randomly divided into those with or  
123 without 7-0 silk ligatures (SUT-S 103, Braintree Scientific, Braintree, MA, USA) around both  
124 maxillary second molars under anesthesia containing 0.4 mg/ml midazolam (LF6476; SANDO, Tokyo,  
125 Japan), 0.3 mg/ml Vetorphale® (Meiji Seika pharma, Tokyo, Japan), 0.03 mg/ml Dorbene® (9021;  
126 Kyouritsu Seiyaku, Tokyo, Japan) to induce experimental periodontitis as previously reported. We did

127 not use female WT and VEIRKO littermates for the study to avoid a potential sexual cycle impact.  
128 After 14 days, the mice were euthanized, and the maxillae were removed for further analysis. All mice  
129 injured by fighting, and mice with lost ligatures were excluded from the study; those who succeeded  
130 in keeping ligatures for 14 days were used for further analysis. To evaluate the alveolar bone loss, left  
131 hemisected maxillae were treated with 0.5% sodium hypochlorite solution for three days, and 3%  
132 hydrogen peroxide for one day. After washing with PBS, the maxillae were stained with 0.05%  
133 Toluidine blue (Muto Pure Chemical, Tokyo, Japan). Periodontal bone loss in defleshed maxillae was  
134 assessed morphometrically using a Leica MZ10 F (Leica-Microsystems, Wetzlar, Germany). Alveolar  
135 bone loss was measured from the cemento-enamel junction (CEJ) of the third mesial root to the  
136 pinnacle of the alveolar bone (AB), and the distal and mesial roots of the second and first molars. The  
137 alveolar bone loss of each group was defined as the sum of distances from the five sites based on a  
138 previous study (Shinjo et al. 2023). For histological assays, right hemisected maxillae were decalcified  
139 for 48 hours using Osteosoft® (Merck, Darmstadt, Germany).

140

#### 141 **Reverse transcriptional quantitative polymerase chain reaction (RT-qPCR)**

142 Total RNA was isolated from gingiva using Trizol® Reagent (Ambion, Waltham, MA, USA), and  
143 reverse transcription was performed using PrimeScript RT Master Mix (TaKaRa Bio, Shiga, Japan).  
144 RT-qPCR was performed using the Luna SYBR® Universal qPCR Kit Master Mix (New England  
145 Biolabs, Ipswich, MA, USA) on a StepOnePlus™ Real-Time System (Applied Biosystems, Carlsbad,  
146 CA, USA) under the following conditions: 95 °C for 3 min, 40 cycles of 95 °C for 3 s, and 60 °C for  
147 30 s. To correct varying copies of first-strand cDNA templates, a passive reference dye (Rox) was  
148 added to the PCR master mix. The results were recorded and analyzed using StepOne™ software  
149 V2.2.2 (Applied Biosystems) utilizing the auto-calculated threshold cycle. The  $\Delta\Delta CT$  method was  
150 used to calculate the relative expression levels of the individual genes, and 18s rRNA was used as an  
151 internal control. The primer sequences used in the present study are described below.

152

#### 153 **Tartrate-resistant acid phosphatase (TRAP) staining and osteoclast quantification**

154 Paraffin-embedded tissues of right hemisected maxillae were cut into 5- $\mu$ m sections and they were  
155 subjected to TRAP/ALP Stain Kit (Fuji-film Wako) according to the manufacturer's instructions.  
156 TRAP positive cells with  $\geq 2$  nuclei on the surface of alveolar bone around the second molar were  
157 counted as active osteoclasts. Photographs were taken using BZ-X800.

158

#### 159 **Immunofluorescent stain**

160 Paraffin-embedded tissues of right hemisected maxillae were cut into 5- $\mu$ m sections and they were  
161 deparaffinized in xylene and rehydrated in graded ethanol solutions. Antigen retrieval was performed  
162 with citrate buffer (pH 6) for 10 min at 95 °C. Sections were rinsed in PBS for 5 min. Non-specific



163 labeling was blocked by incubation with 1% BSA at room temperature for 30 min. Sections were then  
164 incubated with primary antibodies against MPO (ab208670, Abcam) at 4 °C overnight. Then, the  
165 sections were washed and incubated with secondary antibodies for 2 h in the dark at room temperature.  
166 The nucleus was stained using SlowFade Diamond Antifade Mountant with DAPI (Life Technologies,  
167 Waltham, Massachusetts, USA). The samples were visualized by BZ-X800. Positive cells were  
168 quantified using Image J software.

169

### 170 **Hyperglycemia treatment**

171 TKD2 cells were treated with 5.5 mM (low glucose: LG) or 25 mM D-glucose (high glucose: HG) in  
172 DMEM with 0.1% FBS for 48 h before insulin treatment for 10 min to assess the insulin signaling.  
173 For VCAM1 expression and cellular adhesion assays, 48-h LG- or HG-treated TKD2 cells with  
174 DMEM with 0.1% FBS were pretreated with 100 nM insulin or PBS for 30 min. Then, each cell was  
175 stimulated with 10 ng/ml *E. coli* LPS or rmTNF- $\alpha$  for 24 h under the same glucose concentration as  
176 pretreatment. For the osmotic control, 20 mM mannitol was added to TKD2 cells under LG conditions  
177 and incubated for 48 h.

178

### 179 **Intraperitoneal glucose and insulin tolerance test (IPGTT/IPITT)**

180 Intraperitoneal glucose tolerance tests (IPGTTs) and insulin tolerance tests (IPITTs) were performed  
181 as previously reported (Li et al., 2019). Briefly, RD and HFD-fed mice were fasted for 16 h or 6 h  
182 followed by intraperitoneal administration of glucose (2 mg/g body weight) or insulin (0.75 mIU/g  
183 body weight), respectively. Blood was collected from the tail vein for measuring glucose levels at 0,  
184 30, 60, 90 and 120 min after glucose or insulin injection. Blood glucose level was measured using a  
185 Contour glucometer (Bayer, Mishawaka, IN, USA).

186

### 187 **Plasma insulin level measurements**

188 Blood was collected from the tail vein of RD and HFD-fed mice after 16 h of fasting. Plasma insulin  
189 levels were measured using an ELISA kit (Crystal Chem, Elk Grove Village, IL) according to the  
190 manufacturer's protocol.

191

### 192 **Cell transfection**

193 TKD2 cells were plated in 24- or 96-well plates prior to transfection. Cells at approximately 70%  
194 confluency were transfected with the indicated amounts of expression plasmid using 1  $\mu$ L of  
195 Lipofectamine 3000 (Thermo Fisher Scientific), according to the manufacturer's instructions. Cells  
196 were also transfected with a null-expressing pCMV5 vector (RDB05956; RIKEN BioResource  
197 Center) as an empty control vector under the same conditions. FLAG-Foxo1 (pCMV5; Addgene  
198 plasmid #12148; <http://n2t.net/addgene:12148>; RRID: Addgene\_12148) and FLAG-Foxo1-ADA

199 (pCMV5; Addgene plasmid #12149; <http://n2t.net/addgene:12149>; RRID: Addgene\_12149) were gifts  
200 from Dr. Domenico Accili (Naomi Berrie Diabetes Center, Columbia University, New York, USA)  
201 and were obtained from Addgene (Watertown, MA, USA).

202

203 **Statistical analysis/sample size**

204 Based on our pilot study of a ligature-induced bone loss model, we calculated that 6 mice for each  
205 group was the minimum required to detect an overall difference of 0.375 mm bone level with a  
206 standard deviation of 0.21 mm, compared to WT with ligature, with 80% power at the threshold ( $\alpha$ ) of  
207 0.05.

208

209 **Appendix Table 1.** Primers used in this study

210

<b>RT-qPCR</b>	<b>Forward</b>	<b>Reverse</b>
Mouse 18s rRNA	GCTTAATTTGACTCAACACGGGA	AGCTATCAATCTGTCAATCCTGTC
Mouse Tnf $\alpha$	GACAGTGACCTGGACTGTGG	TGAGACAGAGGCAACCTGAC
Mouse Il-1 $\beta$	GAAGAAGAGCCCATCCTCTG	TCATCTCGGAGCCTGTAGTG
Mouse Mcp-1	AGGTCCCTGTGATGCTTCTG	TCTGGACCCATTCTTCTTG
Mouse Vcam1	TCTGAACCCAAACAGAGGCAGAGT	AGCTGGTATCCCATCACTGAGCA
Mouse Icam1	AGATCACATTCACGGTGCTG	CTTCAGAGGCAGGAAACAGG
Mouse E-selectin	GATTGGACACTCAATGGATC	CCTAGACGTTGTAAGAAGGC
Mouse Rankl	CGCTCTGTTCTGTACTTTCG	GAGTCCTGCAAATCTGCGTT
Mouse Opg	CCTTGCCCTGACCACTCTTAT	CACACACTCGGTTGTGGGT
Genotyping		
Mouse VECad F	CCCAGGCTGACCAAGCTGAG	
Mouse Cre R	CCTGGCGATCCCTGAACATG	
Mouse IR flox delta	TCTATCAACCGTGCCTAGAG	
Mouse IR flox F	GATGTGCACCCCATGTCT	
Mouse IR flox R	CTGAATAGCTGAGACCACAG	
Cre26	CCTGGAAAATGCTTCTGTCCG	
Cre36	CAGGGTGTATAAGCAATCCC	

211

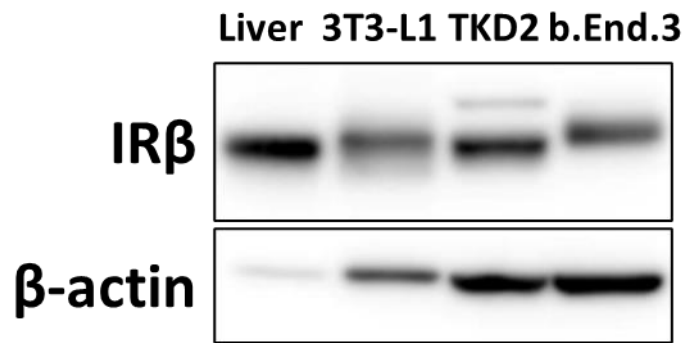
212 All primers were purchased from FASMAC (Kanagawa, Japan).

213 **Appendix Table 2.** Antibodies used in the present study

<b>Product (target)</b>	<b>Supplier/Catalog No.</b>	<b>Host</b>	<b>Dilution</b>
VCAM1	Abcam/ab134047	Rabbit monoclonal	WB: 1:2000
ICAM1	Santa Cruz Biotechnology/sc-8439	Mouse monoclonal	WB: 1:1000
E-selectin	Santa Cruz Biotechnology/sc-137054	Mouse monoclonal	WB: 1:1000
IR $\beta$	Cell Signaling Technology/#3025	Rabbit monoclonal	WB: 1:1000
phospho-Akt (Ser473)	Cell Signaling Technology/#9271	Rabbit polyclonal	WB: 1:1000
total Akt	Cell Signaling Technology/#4691	Rabbit monoclonal	WB: 1:1000
phospho-Erk	Cell Signaling Technology/#4370	Rabbit monoclonal	WB: 1:1000
total Erk	Cell Signaling Technology/#9102	Rabbit polyclonal	WB: 1:1000
phospho-FoxO1 (Thr24)/FoxO3a (Thr32)	Cell Signaling Technology/#9464	Rabbit polyclonal	WB: 1:1000
total FoxO1	Cell Signaling Technology/#2880	Rabbit monoclonal	WB: 1:1000
$\beta$ -actin	Fuji-film Wako/010-27841	Mouse monoclonal	WB: 1:1000
HRP-linked anti-mouse IgG	Cell Signaling Technology /#7076	Horse	WB: 1:5000
HRP-linked anti-Rabbit IgG	Cell Signaling Technology /#7074	Goat	WB: 1:5000
IgG2a kappa Isotype Control	Thermo Fisher Scientific/14-4321-82	Rat monoclonal	Neu: 10 $\mu$ g/ml
VCAM1	Thermo Fisher Scientific/14-1061-82	Rat monoclonal	Neu: 10 $\mu$ g/ml
ICAM1	Thermo Fisher Scientific/14-0541-82	Rat monoclonal	Neu: 10 $\mu$ g/ml
E-selectin	Thermo Fisher Scientific/ MA1-06507	Rat monoclonal	Neu: 10 $\mu$ g/ml
Myeloperoxidase	Abcam/ab208670	Rabbit monoclonal	IF: 1:100
Anti-rabbit IgG conjugated with Alexa Flour® 488	Abcam/ab150077	Goat	IF: 1:200
CD31	Bio Legend/102402	Mouse monoclonal	IF: 1:200
IR $\beta$	Cell Signaling Technology/ #23413	Rabbit monoclonal	IF: 1:100
Anti-mouse IgG conjugated with Alexa Flour® 562	Jackson ImmunoResearch/415-605-166	Rat monoclonal	IF: 1:200

214 WB: Western blotting, Neu: Neutralization, IF: Immunofluorescence

215 **Appendix figures**



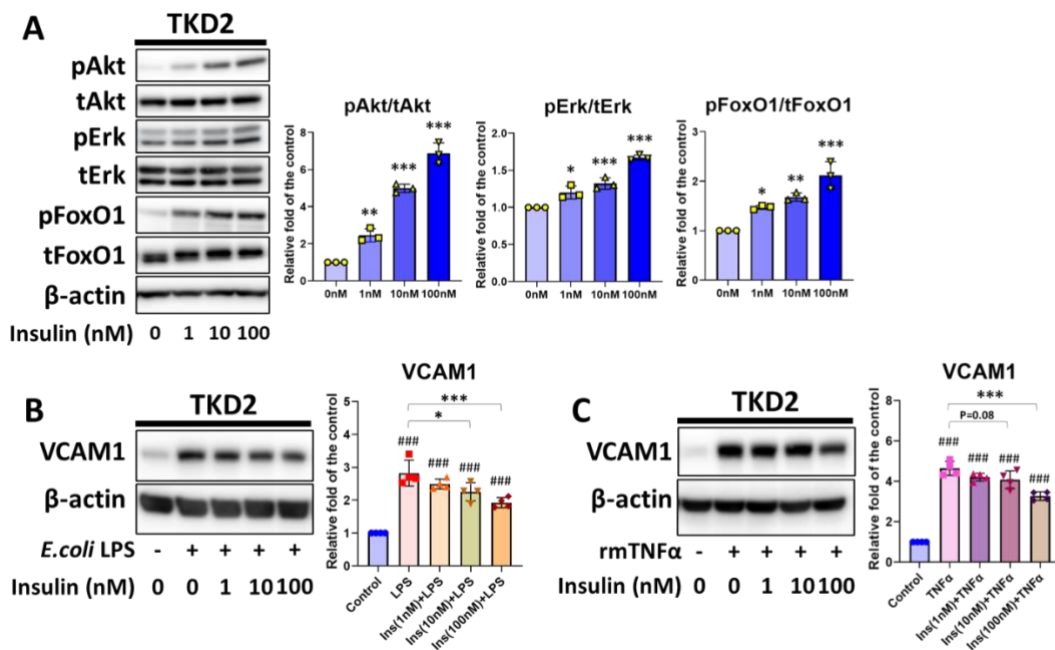
216

217 **Appendix Figure 1 Confirmation of IRβ expression in TKD2 and b.End.3 cells.**

218 Western blotting of IRβ in lean mouse livers, mature adipocytes (differentiated 3T3-L1 cells), TKD2  
219 cells, and b.End.3 cells.

220

221



222

223 **Appendix Figure 2 Insulin action in TKD2 cells in dose-dependent manner.**

224 (A) Insulin-induced phosphorylation of Akt, Erk and FoxO1 in TKD2 cells in dose-dependent manner

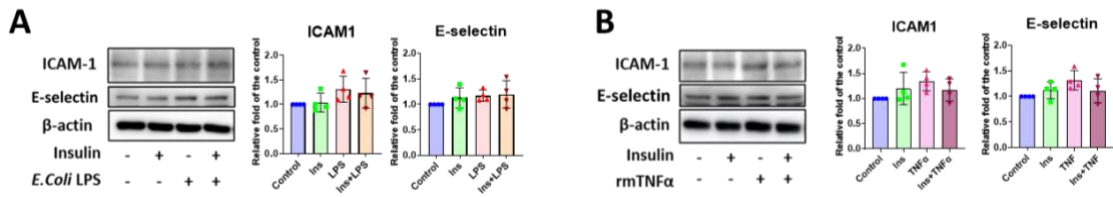
225 (1-100 nM) (n = 3). (B and C) VCAM1 expression in TKD2 cells stimulated with 10 ng/ml LPS or

226 TNFα for 24 h with or without 1-100 nM insulin pretreatment for 30 min (n = 4). \* p<0.05, \*\* p<0.01,

227 \*\*\* p<0.001. ### p<0.001 vs Control. All individual data are shown in a scatter plot. Representative

228 western blotting is shown. Data are shown as mean ± SD.

229



230

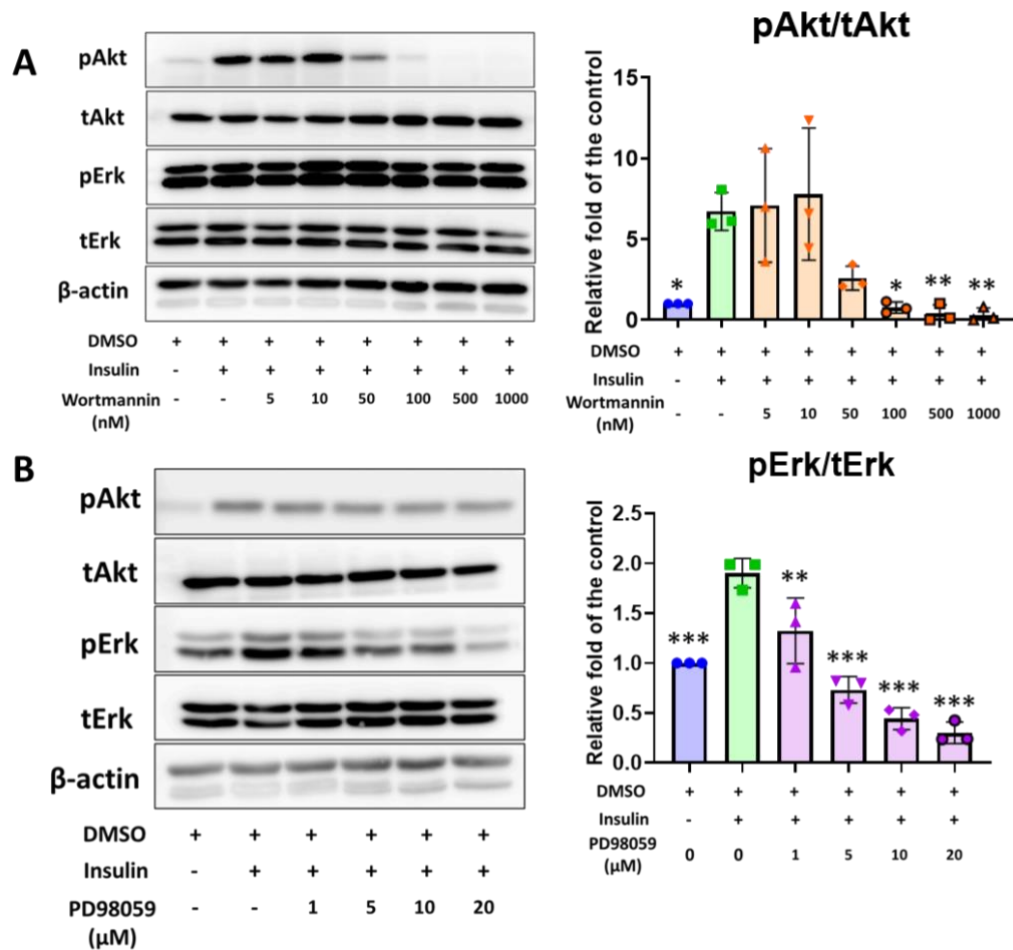
231

232 **Appendix Figure 3 ICAM1 and E-selectin expression in TKD2 cells with LPS or insulin**  
 233 **stimulation.**

234 (A) ICAM1 and E-selectin in TKD2 cells with or without insulin (100 nM) pretreatment for 30 min  
 235 or LPS (10 ng/ml) stimulation. (B) ICAM1 and E-selectin in TKD2 cells with or without insulin (100  
 236 nM) pretreatment for 30 min or TNFα (10 ng/ml) stimulation. Cells were stimulated with LPS or TNFα  
 237 for 24 h (n = 4). All individual data are shown in a scatter plot. Representative western blotting is  
 238 shown. Data are presented as mean ± SD.

239

240



241

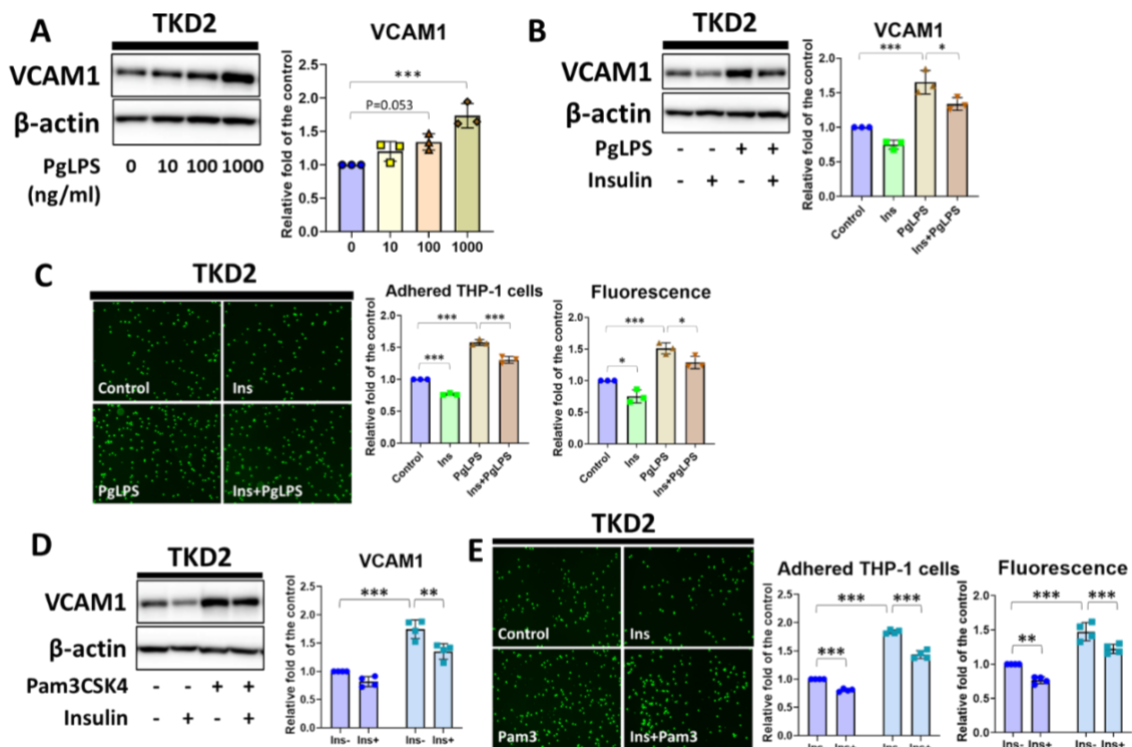
242 **Appendix Figure 4 Confirmation of working concentrations of wortmannin and PD98059 in**  
 243 **insulin-treated TKD2 cells.**

244 (A) Akt and Erk phosphorylations in TKD2 cells stimulated with insulin (100 nM) in the presence or  
 245 absence of wortmannin at indicated concentrations. (B) Akt and Erk phosphorylations in TKD2 cells  
 246 stimulated with insulin (100 nM) in the presence or absence of PD98059 at indicated concentrations.  
 247 Cells were treated with insulin for 10 min after pretreatment of each inhibitor for 30 min.

248 \*  $p < 0.05$ , \*\*  $p < 0.01$ , \*\*\*  $p < 0.001$  vs DMSO + insulin ( $n = 3$ ). Representative western blotting is  
 249 shown. Mean  $\pm$  SD are shown in the bar graph.

250





251

252

**Appendix Figure 5 Confirmation of the inhibitory effect of insulin on VCAM1 expression and cellular adhesion with leukocytes in PgLPS- or Pam3CSK4-treated TKD2 cells.**

253

(A) PgLPS-induced VCAM1 expression in TKD2 cells in a dose-dependent manner (10-1000 ng/ml).

255

(B and C) VCAM1 expression and cellular adhesion with THP-1 cells in TKD2 cells treated with 1000 ng/ml PgLPS for 24 h with or without 100 nM insulin pretreatment for 30 min.

256

257

(D and E) VCAM1 expression and cellular adhesion with THP-1 cells in TKD2 cells treated with 100 ng/ml Pam3CSK4 for 24 h with or without 100 nM insulin pretreatment for 30 min. \*  $p < 0.05$ , \*\*  $p < 0.01$ , \*\*\*  $p < 0.001$

258

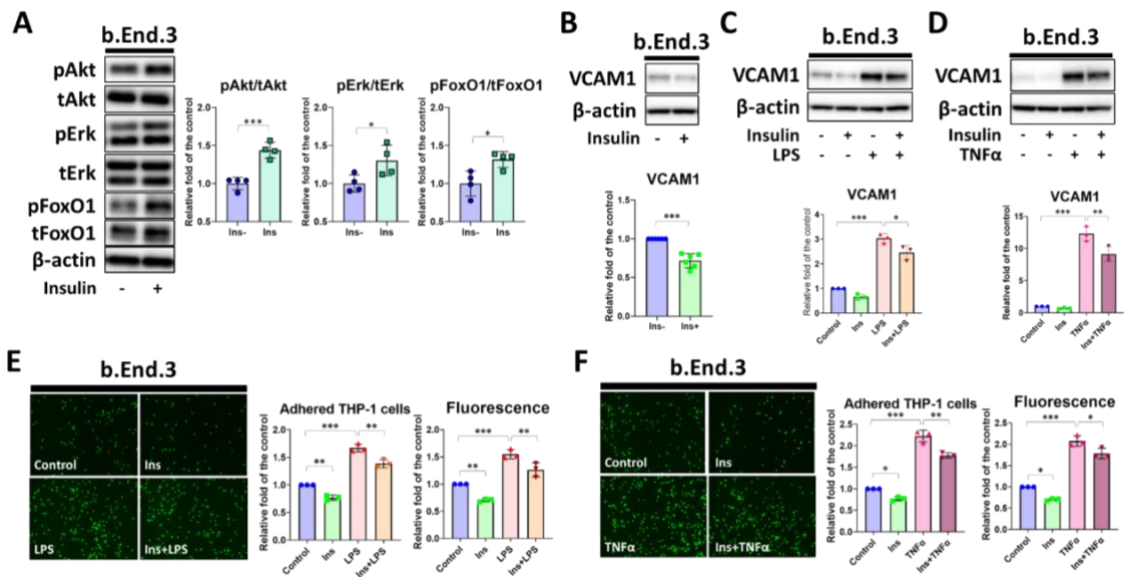
259

( $n=3-4$ ). All individual data are shown in a scatter plot. Representative western blotting and microscopy photos are shown. Data are presented as mean  $\pm$  SD.

260

261

262



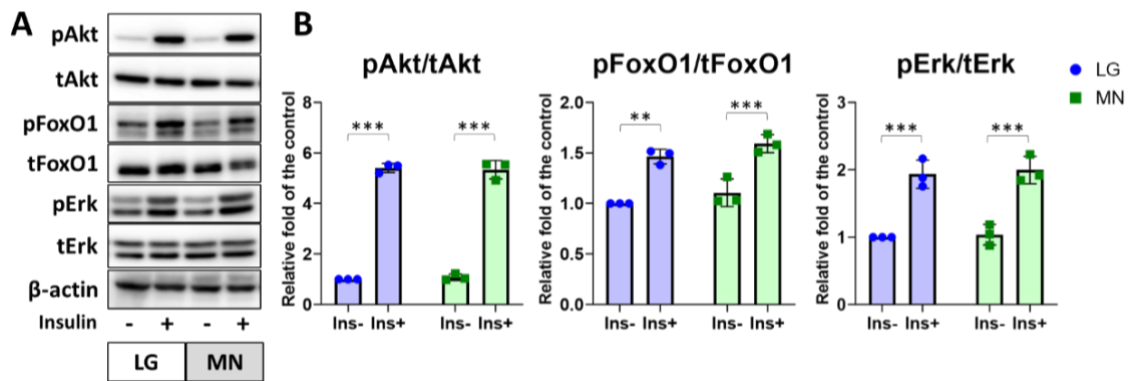
263

264 **Appendix Figure 6 Confirmation of the inhibitory effect of insulin on VCAM1 expression and**  
 265 **cellular adhesion with leukocytes in LPS- or TNF $\alpha$ -treated b.End.3 cells.**

266 (A) 100 nM insulin-induced phosphorylation of Akt, Erk and FoxO1 in b.End.3 cells. (B) VCAM1  
 267 expression levels in b.End.3 cells with PBS or 100 nM insulin for 24 h. (C and D) 24 h of LPS- or  
 268 TNF $\alpha$  treatment-induced VCAM1 expression in b.End.3 cells with or without 100 nM insulin  
 269 pretreatment for 30 min. (E and F) Cellular adhesion with THP-1 cells in b.End.3 cells treated with 10  
 270 ng/ml of LPS or TNF $\alpha$  for 24 h with or without 100 nM insulin pretreatment for 30 min. \* p<0.05, \*\*  
 271 p<0.01, \*\*\* p<0.001 (n = 3-4). All individual data are shown in a scatter plot. Representative western  
 272 blotting and microscopy photos are shown. Data are presented as mean  $\pm$  SD.

273

274



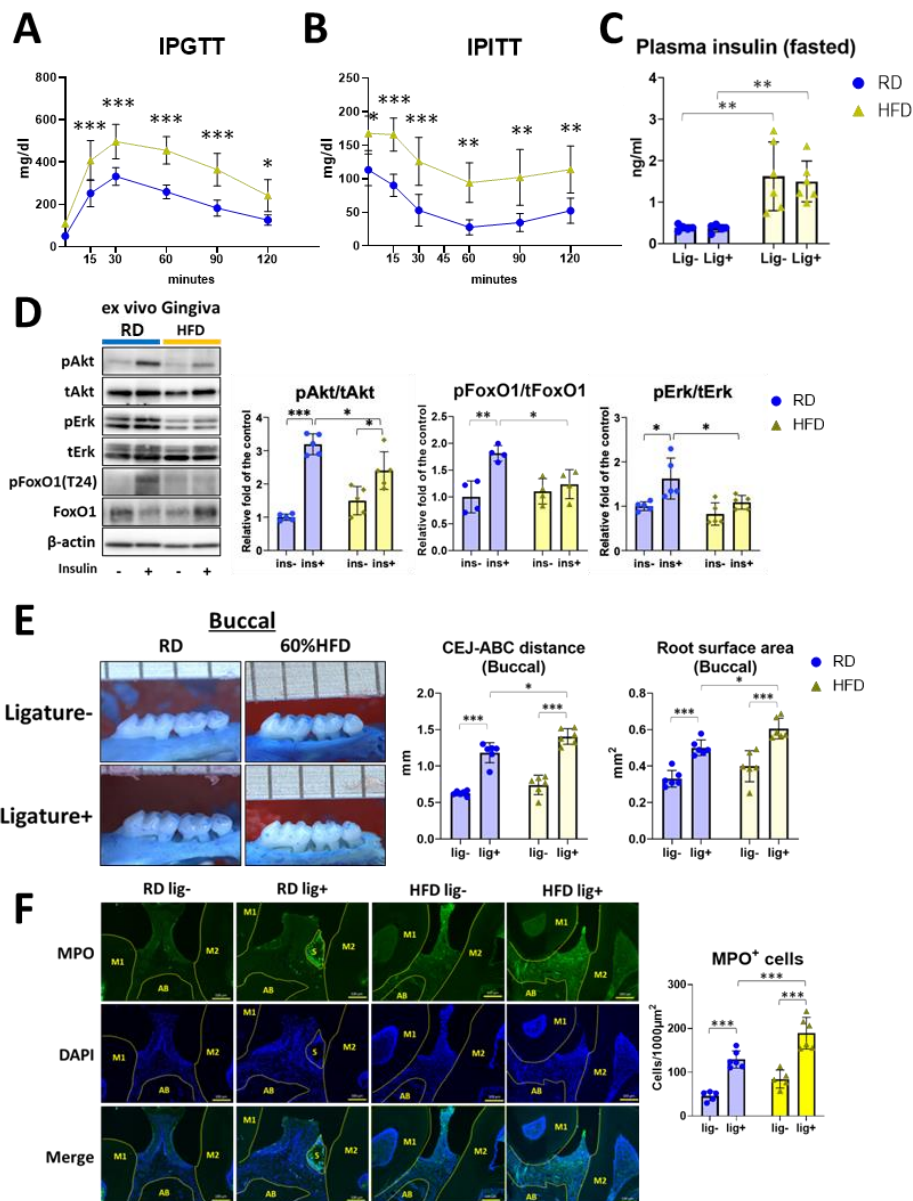
275

276 **Appendix Figure 7 Confirmation of insulin signaling in TKD2 cells under LG plus 20 mM**  
 277 **mannitol.**

278 (A-B) Phosphorylations of Akt, FoxO1 and Erk in TKD2 cells stimulated with insulin (100 nM) for  
 279 10 min under preincubation with 48 h of euglycemia (5.5 mM D-glucose: LG) and an osmotic control  
 280 (5.5 mM D-glucose + 20 mM mannitol: MN). \*\*  $p < 0.01$ , \*\*\*  $p < 0.001$  ( $n = 3$ ). All individual data are  
 281 shown in a scatter plot. Representative western blotting and microscopy photos are shown. Data are  
 282 presented as mean  $\pm$  SD.

283

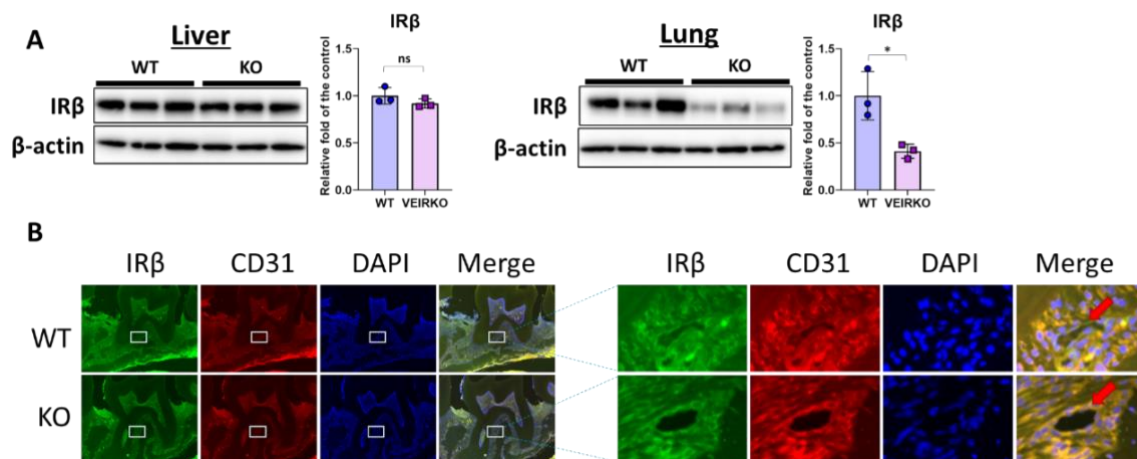
284



285

286 **Appendix Figure 8 HFD-fed mice showed downregulation of insulin-mediated phosphorylation**  
 287 **of FoxO1 in the gingiva and exacerbation of ligature-induced alveolar bone loss.**

288 (A) Blood glucose levels during IPGTT and (B) IPITT in RD and HFD-fed mice. (C) Plasma insulin  
 289 levels in RD and HFD-fed mice fasted for 16 h. (D) Insulin signaling in the gingiva from the regular  
 290 diet (RD) and HFD-fed mice with *ex vivo* insulin (100 nM) stimulation for 10 min. (E) Assessment of  
 291 alveolar bone loss in RD- and HFD-fed mice with or without ligature for 14 days. (F) Detection of  
 292 MPO-positive cells in periodontal tissue of RD- and HFD-fed mice with or without ligature for 14  
 293 days. \*  $p < 0.05$ , \*\*  $p < 0.01$ , \*\*\*  $p < 0.001$  ( $n = 4-6$ ). All individual data are shown in a scatter plot.  
 294 Representative western blotting and microscopy photos are shown. Data are presented as mean  $\pm$  SD.  
 295



296

297 **Appendix Figure 9 Comparison of IRβ expression in the lung, liver and periodontal tissues.**

298 (A) Representative blots of IRβ in the livers and lungs from WT and VEIRKO mice (n=3). (B)

299 Representative photos of immunofluorescent staining of IRβ in the ECs of periodontal tissue from WT

300 and VEIRKO mice. Red arrows indicate the microvascular. \* p<0.05. All individual data are shown in

301 a scatter plot. Representative western blotting and microscopy photos are shown. Data are presented

302 as mean ± SD.

303

304

305 **References**

- 306 Kitamoto S, Nagao-Kitamoto H, Jiao Y, Gilliland MG 3rd, Hayashi A, Imai J, Sugihara K, Miyoshi  
307 M, Brazil JC, Kuffa P et al. 2020. The Intermucosal Connection between the Mouth and Gut in  
308 Commensal Pathobiont-Driven Colitis. *Cell*. 182(2):447-462.e14.
- 309 Li Q, Fu J, Xia Y, Qi W, Ishikado A, Park K, Yokomizo H, Huang Q, Cai W, Rask-Madsen C et al.  
310 2019. Homozygous receptors for insulin and not IGF-1 accelerate intimal hyperplasia in insulin  
311 resistance and diabetes. *Nat Commun*. 10(1):4427.
- 312 Shinjo T, Onizuka S, Zaito Y, Ishikado A, Park K, Li Q, Yokomizo H, Zeze T, Sato K, St-Louis R, et  
313 al. 2023. Dysregulation of CXCL1 expression and neutrophil recruitment in insulin resistance and  
314 diabetes-related periodontitis in male mice. *Diabetes*. db221014, in press.
- 315 Shinjo T, Nakatsu Y, Iwashita M, Sano T, Sakoda H, Ishihara H, Kushiya A, Fujishiro M,  
316 Fukushima T, Tsuchiya Y, et al. 2015. DPP-IV inhibitor anagliptin exerts anti-inflammatory effects on  
317 macrophages, adipocytes, and mouse livers by suppressing NF- $\kappa$ B activation. *Am J Physiol*  
318 *Endocrinol Metab*. 309(3):E214-223.